Energy 326 (2025) 136101

Contents lists available at ScienceDirect

Energy

journal homepage: www.elsevier.com/locate/energy

Long-term climate change effects on power performance of wave energy converters: A case study

Kumars Mahmoodi [a,*], Hossein Rezaie Fard [b], Jari Böling [c]

[a] Faculty of Natural Sciences and Engineering, Åbo Akademi University, Turku, Finland
[b] Department of Civil Engineering, Persian Gulf University, Iran
[c] Department of Mechanical and Materials Engineering, University of Turku, Finland

ARTICLE INFO

Keywords:
Wave energy converter
WEC array modeling
Power performance
Long-term analysis
Climate change impact
ERA5 data set

ABSTRACT

The power performance of wave energy converters (WECs) is directly related to the characteristics of ocean waves, which are influenced by climate change through variations in wave height, frequency, direction, and storm intensity. This study investigates the impacts of long-term sea state climate variability on the power performance of single-body heaving point absorber WEC arrays through a case study of four geographically diverse regions: the Western Tropical Pacific, Southwest Indian Ocean, North Pacific, and South Atlantic. The trends and evaluation of wave energy availability, along with the power absorption of four WEC array configurations across different temporal and spatial resolutions, are analyzed using the ERA5 European Centre for Medium-Range Weather Forecasts (ECMWF) historical hourly wave condition dataset from 1940 to 2023. The results highlight regional differences in the effects of climate change on wave energy potential and WEC power performance. Statistical methods, including the Mann–Kendall trend test, are employed to quantify trend magnitude and direction. Despite an overall increase in absorbed power due to climate-driven changes in wave patterns, observed trends in CWR and q-factor are not uniformly positive, highlighting the complex influence of wave-structure interactions and inconsistent wave climates. This analysis underscores the importance of understanding both spatial and temporal changes in wave conditions when optimizing WEC array layouts for sustained, efficient energy capture in a changing climate.

1. Introduction

As global energy demands continue to increase and concerns about climate change intensify, the search for reliable, renewable energy sources has become a priority [1,2]. Ocean wave energy presents a promising and largely untapped potential among these sources [3,4]. WECs are devices designed to harness the kinetic energy of ocean waves. However, the long-term performance of WECs may be influenced by changing climate conditions [5]. It is necessary to understand how climate change impacts the availability and characteristics of wave energy resources. Climate change is expected to alter oceanographic conditions, including wave height, period, and direction, which are critical factors for the power generation capacity of WECs [6,7]. Regions of the world can experience significant variations in wave energy potential, which impacts the efficiency and reliability of wave energy systems. The ability of WECs to adapt to these changes will be essential for ensuring their long-term viability as a part of the global renewable energy solution [8].

Climate change can affect the amount of harvested power by WECs through its impact on key oceanographic factors that determine wave energy potential [9]. The primary effects include changes in wave height, wave frequency, wave direction, and storm intensity [10–12]. The energy harvested by WECs is proportional to the square of the wave height [13]. This means even small changes in wave height can significantly affect the generated power. As the climate changes, certain regions may experience either increases or decreases in average wave heights. Changes in wind patterns, a direct consequence of climate change, can alter wave frequency [14,15]. This could either enhance or reduce the effectiveness of WECs, depending on whether the changes align with their optimal operating conditions. Changes in wind patterns due to climate change can also alter wave direction [16]. If waves begin coming from a direction that the WEC is not optimized for, the amount of harvested energy may decrease unless the system can adapt.

Climate change is likely to increase or decrease the frequency and intensity of storms in some regions [17]. This can lead to more frequent shutdowns or damage to WECs in areas with severe storms, reducing long-term power output [18]. Alternatively, calmer seas may also reduce the available wave energy in regions where storm intensity

* Corresponding author.
E-mail addresses: kumars.mahmoodi@abo.fi (K. Mahmoodi), hosseinrezaefard@mehr.pgu.ac.ir (H.R. Fard), jari.boling@utu.fi (J. Böling).

https://doi.org/10.1016/j.energy.2025.136101
Received 11 December 2024; Received in revised form 17 March 2025; Accepted 10 April 2025
Available online 26 April 2025

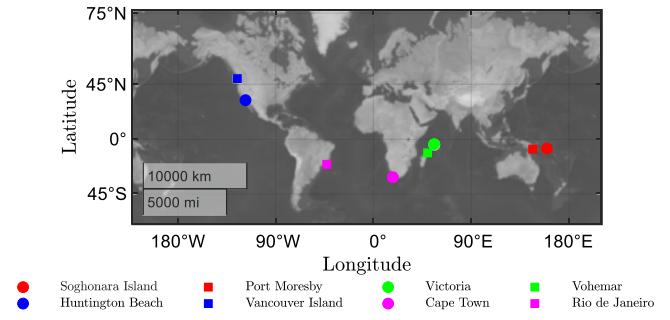

Fig. 1. Geographical locations of the considered points to study the power performance of case study WEC arrays.

decreases [19]. Rising sea levels can change the depth and profile of wave propagation as they reach coastal areas which are the place where WECs are installed. Deeper water might enhance or reduce the efficiency of certain WEC designs depending. As sea levels rise due to global warming [20,21], WECs installed in shallow coastal waters may experience altered wave dynamics, potentially reducing their efficiency [22]. Seasonal and long-term climate variability can cause fluctuations in wave energy potential [23]. This may create challenges for grid stability and reliability of energy supply from WECs.

Some studies related to the effects of long-term climate change on wave energy resources and WECs' performance have been conducted in past years. Research [24] introduced a method to measure the impacts of climate change on wave energy generation by a WEC. When applied to the Wave Hub site off Cornwall, it suggested that future wave conditions will slightly increase or decrease available wave power and energy yield, depending on greenhouse gas emission scenarios. Studies [25,26] have shown that rising upper-ocean temperatures and shifting wind patterns have contributed to a measurable increase in global wave power, with regional variations in its impact. The study [27] analyzed the 20th-century wave energy resource trends off the west coast of Ireland. It concluded a 40% increase over the century and significant increases in the last 20 years. It highlighted the impact of these variations on the power absorption of WECs and noted a rise in extreme events. The key studies on the impacts of climate change on various renewable energy sources were reviewed in [10]. It highlighted research gaps, especially in specific regions and technologies, and underscored the need for economic estimates with a value chain perspective.

Ref. [28] summarized key scientific works from the 2018 SEEP conference, focusing on renewable energy and environmental protection. It includes advances in energy conversion systems, policies for renewable energy adoption, greenhouse gas emission reductions, and CO_2 capture progress. Study [29] investigated how climate change affects wave energy potential along the Atlantic coast of the Iberian Peninsula. According to this research, high-emission global warming scenarios show a decreasing trend in wave power, especially in the northwest, with slight increases near the Strait of Gibraltar. The long-term variability in global wave power was evaluated in [30] using the ERA5 wave reanalysis data (1940–2022). Findings showed a consistent increase in wave power which is driven by climate change and Antarctic Oscillation events. These changes were especially significant in the Southern Hemisphere, affecting mid and low-latitude regions of the oceans.

Ref. [18] examined how long-term changes in wave climate affect oscillating water column WECs in the Mediterranean. According to this research, projected wave climate changes by year 2100 show significant regional variations in optimal device geometry and potential increases in annual energy production. Study [15] investigated the impact of long-term variations in wave periods on the WECs performance from 1900 to 2010. Using reanalysis data (ERA-20C and ERA5). It found significant changes in wave periods globally and at specific locations like Ireland. The findings reveal that performance variations of up to 20% occur for oscillating water column devices and floating bodies due to deviations from their natural resonance frequency or optimal wave period.

In recent years, Artificial Intelligence (AI) has revolutionized the wave energy by improving the efficiency, control, and reliability of WECs. AI techniques are extensively employed to optimize wave energy extraction [31–33] and prediction of wave conditions [34–37]. For instance, a time-series auto-regressive model was applied to predict wave excitation force in the near future [38]. The paper [39] presented a Meta-learner gradient boosting method to improve wave energy prediction accuracy, leveraging multi-layer convolutional dense neural networks and optimized extreme gradient boosting. Study [40] integrated parallelized deep reinforcement learning and computational fluid dynamics to control a point absorber WEC by dynamically adjusting the PTO force based on the wave features. These advancements indicate the pivotal role of AI in wave energy by allowing intelligent decision-making, optimizing energy conversion, and enhancing resilience against climate change wave variability [41].

The literature review clearly shows that comprehensive and diverse research on how climate change affects the performance of WECs is still lacking and more research is needed in this field. While several studies have investigated WEC performance, most focus on short-term analyses, typically spanning a few years. It is crucial to understand how climate change-induced variations in wave characteristics influence power performance over multiple decades. Existing research primarily evaluates individual WEC performance or simple array configurations without considering how different array layouts respond to climate change. Given that array interactions can significantly impact power absorption and overall efficiency, it is essential to analyze how various configurations perform under evolving wave conditions. Moreover, Many prior assessments focus on a limited number of locations, often in European or North American waters. However, climate change effects on wave energy resources vary significantly across different ocean basins. The long-term effects of climate change on wave energy resources and the power performance of WEC arrays remain insufficiently understood.

This study aims to investigate the potential impacts of long-term climate variability on the power performance of single-body heaving point absorber WEC arrays in selected ocean regions from 1940 to the end of 2023 based on the ERA5 ECMWF reanalysis data set [42]. By focusing on four diverse regions – the Western Tropical Pacific, the Southwest Indian Ocean, the North Pacific, and the South Atlantic – this research provides insight into how different geographical locations may have experienced changes in wave energy resources over the past decades. These analyses focus on the interaction between changing climate variables (Significant height of combined wind waves and swell, Peak wave period, and Mean wave direction) and the operational efficiency of WEC arrays. To do this purpose, several analytical approaches are conducted: a comprehensive analysis of historical wave climate data to identify trends and changes in wave patterns of the considered studied area, simulation of four different types of single-body heaving point absorber WEC arrays, assessing how different wave conditions impact considered WEC arrays' efficiency using existing WEC power performance criteria that relate wave parameters to power generation, including annual, seasonal, and extreme event performance metrics, and finally use statistical metrics, graphs, and tables to compare WEC performance across different climate scenarios.

Understanding these trends is crucial for optimizing WEC designs to ensure resilience against climate-driven changes. This research contributes to the broader goal of integrating wave energy into future renewable energy strategies, offering valuable insights for policymakers, engineers, and researchers working to secure a sustainable energy future in a changing climate. In general, the necessity of conducting this research can be listed as follows:

- Understanding how long-term climate changes might affect WECs ensures that future energy planning and infrastructure development remain robust, adaptable, and economically viable.

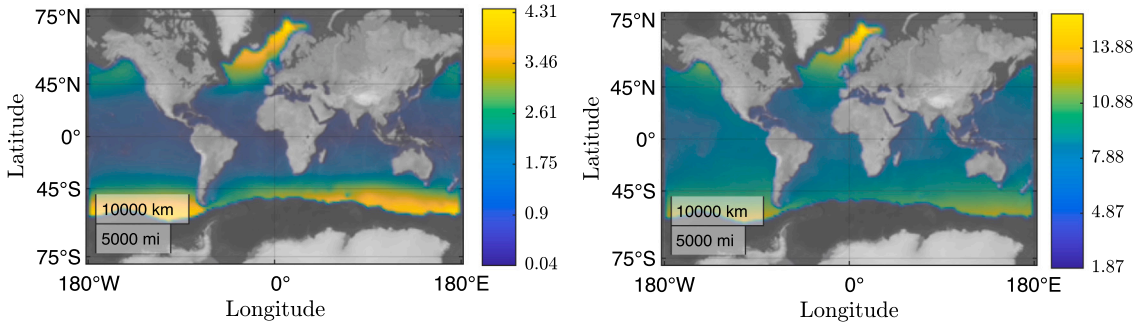

(a) Significant height of wind waves and swell (b) Peak wave period

Fig. 2. The overall hourly mean of ERA5 collected data for the world's significant wave height and peak wave period from 1940 to 2023.

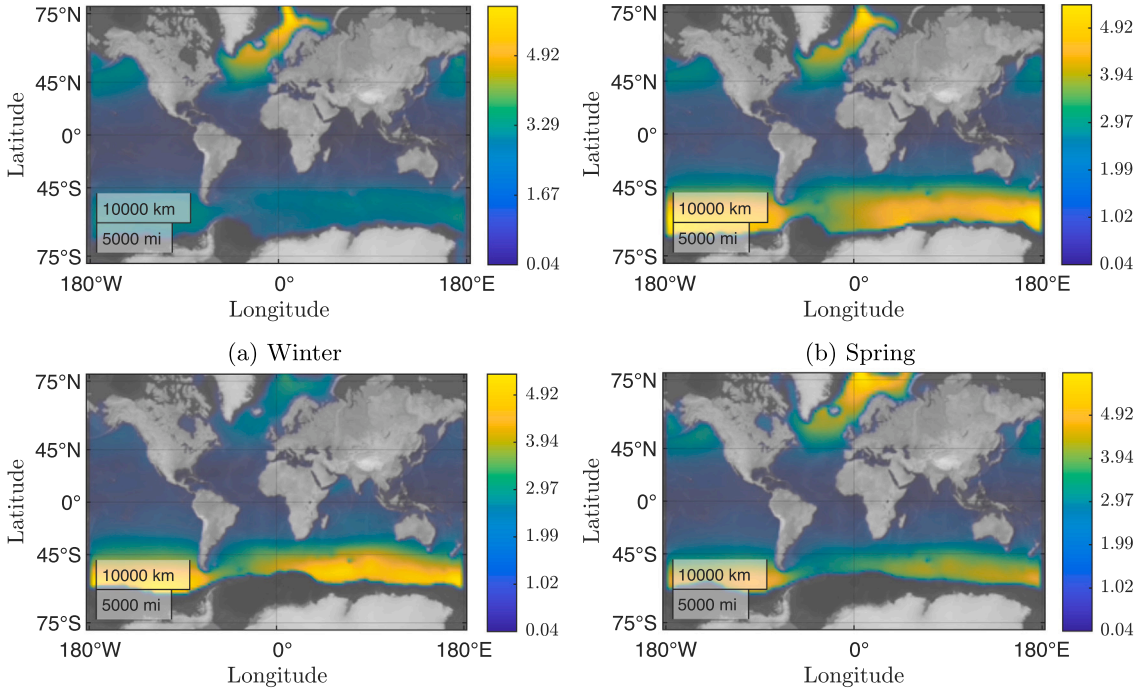

(a) Winter (b) Spring

(c) Summer (d) Autumn

Fig. 3. The overall hourly mean of ERA5 collected data for the world's significant wave height of different seasons from 1940 to 2023.

- Climate change can alter critical sea state parameters such as wave height and period. All these parameters directly influence the efficiency and performance of WECs. Assessing these changes helps anticipate and adapt to future variations in energy output, which reduces uncertainties in energy supply from WECs.
- Investigating long-term climate impacts on WECs allows engineers and designers to build more adaptive systems capable of maintaining performance even as climate patterns change. This ensures the long-term sustainability and reliability of wave energy projects.
- By studying specific locations, such as the Western Tropical Pacific or South Atlantic (as in this study), it is possible to design wave energy systems to optimize performance in specific climates. This geographical focus enhances understanding of region-specific challenges and opportunities.
- Studying the interplay between climate change and WEC performance fills gaps in understanding how ocean energy systems might evolve over the coming decades.
- By understanding the climate's evolving impact on energy infrastructure like WECs, governments can create better policies and financial models that promote sustainable energy development over the next few decades.

The novelty of this study lies in its comprehensive, long-term assessment of WEC array performance under climate-driven wave variations, which has not been extensively explored in previous research. Unlike most studies that focus solely on changes in wave energy potential, this work explicitly examines how these changes affect power performance metrics, such as capture width ratio (CWR) and q-factor, across different WEC array layouts. Additionally, this research employs a high-resolution historical dataset (ERA5,1940–2023) and apply statistical trend analysis to evaluate spatial and temporal variations in wave energy conversion. This study uniquely highlights how site-specific wave-structure interactions influence efficiency trends. By bridging climate science and wave energy engineering, this research provides new insights into optimizing WEC arrays for long-term resilience in a changing climate.

Other remaining parts of the manuscript are as follows: Section 2 presents the used methods and materials, starting with the selection of study areas (Section 2.1), followed by the considered wave climate

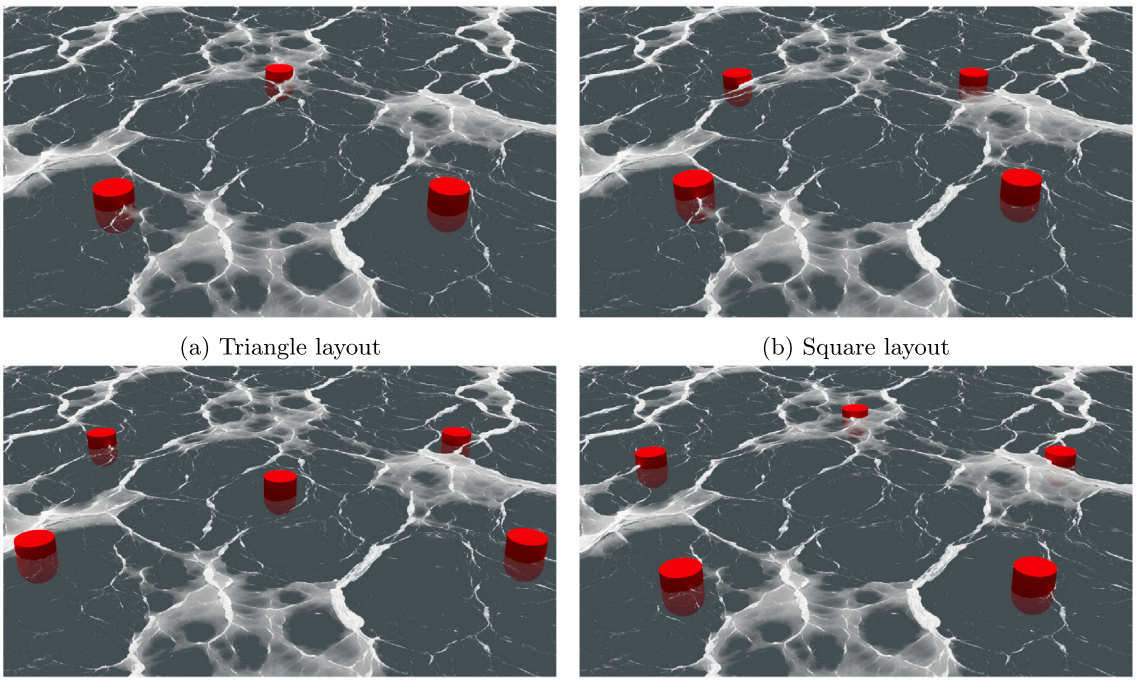

(a) Triangle layout (b) Square layout

(c) Rectangular Layout with a WEC in the Middle (d) Pentagon layout

Fig. 4. Schematic representation of the considered WEC array layouts.

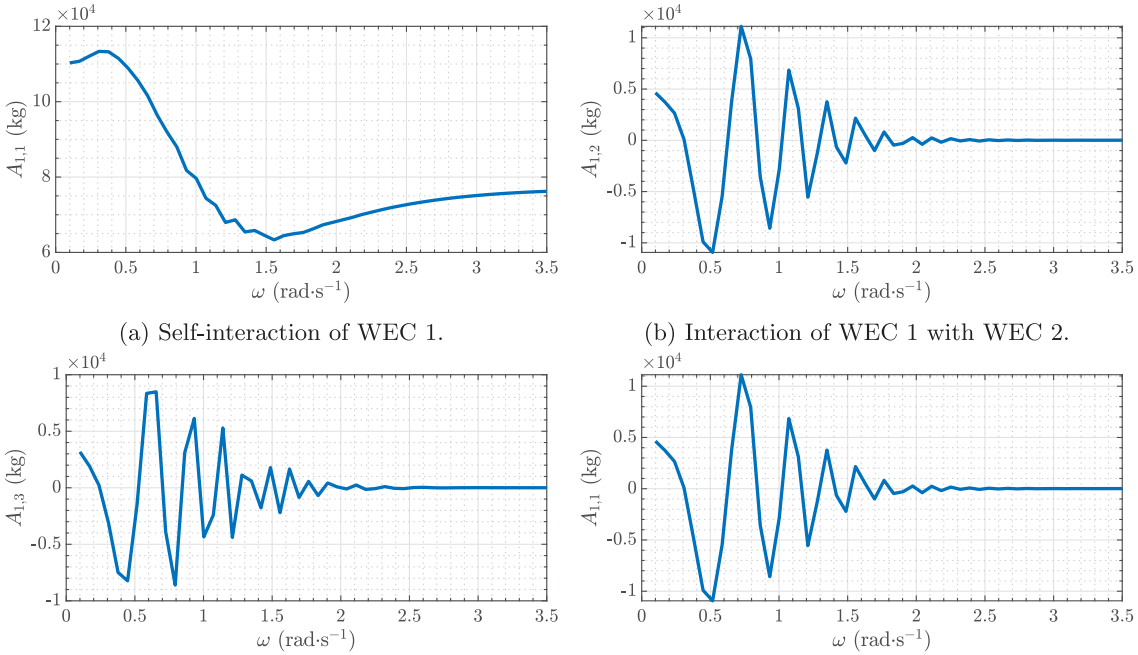

(a) Self-interaction of WEC 1. (b) Interaction of WEC 1 with WEC 2.

(c) Interaction of WEC 1 with WEC 3. (d) Interaction of WEC 1 with WEC 4.

Fig. 5. Calculated added mass coefficients in the heave direction for WEC 1 (upper right corner) of Layout 2 (square layout) and its interaction with other WECs.

data from the ERA5 reanalysis dataset (Section 2.2), and explanation of different WEC array layouts (Section 2.3). Section 3 outlines the governing equation of motion of the WEC arrays, capturing the dynamic interactions between the devices and the wave environment. In Section 3.1, the power performance metrics are introduced which provides a framework for evaluating the efficiency and effectiveness of the WEC arrays under long-term wave conditions. The results of the analyses are presented in Section 4, followed by the conclusions drawn from this study in Section 5.

2. Methods and materials

This section outlines the methodology and the materials used in this research. The study focuses on several regions with diverse wave climates using historical wave data from the ERA5 reanalysis. The WEC

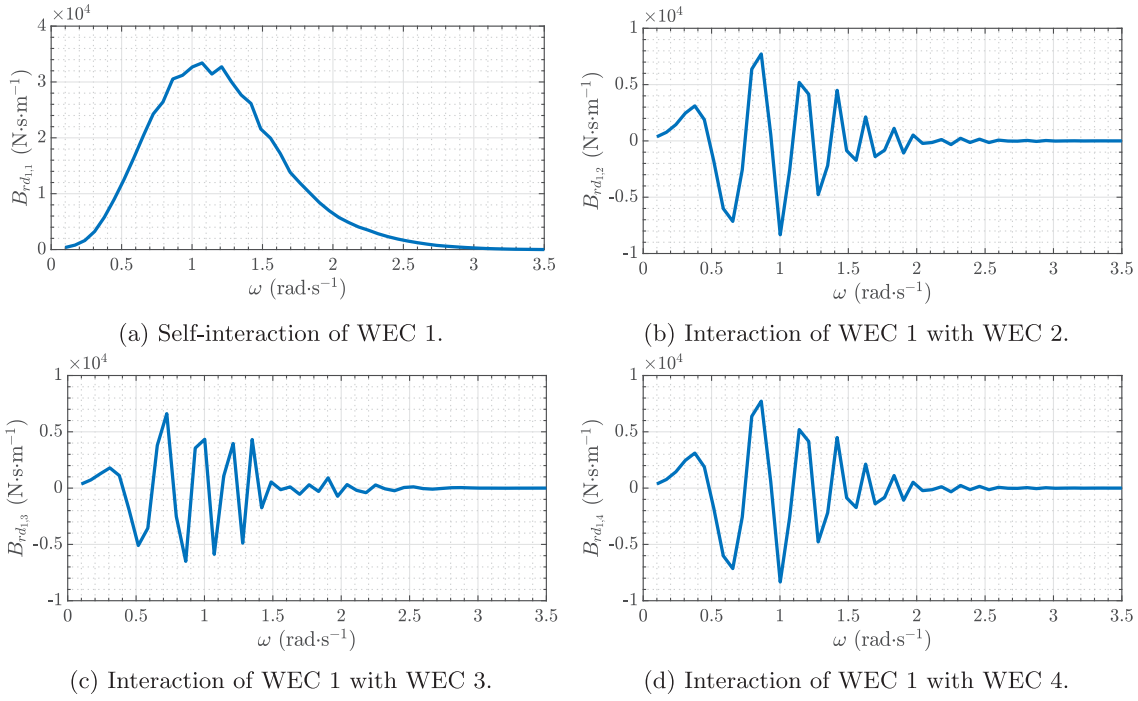

(a) Self-interaction of WEC 1. (b) Interaction of WEC 1 with WEC 2.

(c) Interaction of WEC 1 with WEC 3. (d) Interaction of WEC 1 with WEC 4.

Fig. 6. Calculated radiation wave damping coefficients in the heave direction for WEC 1 (upper right corner) of Layout 2 (square layout) and its interaction with other WECs.

H_s (m) \ T_p (s)	4	4.5	5	5.5	6	6.5	7	7.5	8	8.5	9	9.5	10	10.5	11	11.5	12	12.5	13	13.5	14	14.5	15
8	32.1	53.43	79.96	110.1	142.5	173.5	200.2	226.6	254.9	281.2	289.6	305.2	319.6	325.1	318.3	324.3	331.5	333.8	338.2	337.8	334.2	336.4	336.9
7.5	28.22	46.96	70.28	96.77	125.2	152.5	176	199.1	224.1	247.1	254.5	268.3	280.9	285.7	279.8	285	291.4	293.4	297.3	296.9	293.7	295.6	296.1
7	24.58	40.9	61.22	84.29	109.1	132.8	153.3	173.5	195.2	215.3	221.7	233.7	244.7	248.9	243.7	248.3	253.8	255.6	258.9	258.7	255.9	257.5	258
6.5	21.19	35.27	52.78	72.68	94.07	114.5	132.2	149.6	168.3	185.6	191.2	201.5	211	214.6	210.1	214.1	218.8	220.4	223.3	223	220.6	222.1	222.4
6	18.06	30.05	44.98	61.93	80.16	97.57	112.6	127.5	143.4	158.2	162.9	171.7	179.8	182.8	179.1	182.4	186.5	187.8	190.2	190	188	189.2	189.5
5.5	15.17	25.25	37.79	52.04	67.35	81.99	94.64	107.1	120.5	132.9	136.9	144.3	151.1	153.6	150.4	153.3	156.7	157.8	159.9	159.7	158	159	159.3
5	12.54	20.87	31.23	43.01	55.66	67.76	78.21	88.51	99.59	109.8	113.1	119.2	124.8	127	124.3	126.7	129.5	130.4	132.1	132	130.6	131.4	131.6
4.5	10.16	16.9	25.3	34.84	45.09	54.89	63.35	71.69	80.67	88.96	91.63	96.58	101.1	102.8	100.7	102.6	104.9	105.6	107	106.9	105.8	106.4	106.6
4	8.03	13.36	19.99	27.52	35.62	43.37	50.06	56.64	63.74	70.29	72.4	76.31	79.89	81.27	79.58	81.07	82.88	83.46	84.55	84.46	83.55	84.09	84.24
3.5	6.14	10.23	15.3	21.07	27.28	33.2	38.33	43.37	48.8	53.82	55.43	58.43	61.17	62.22	60.93	62.07	63.45	63.9	64.74	64.66	63.97	64.38	64.49
3	4.51	7.51	11.24	15.48	20.04	24.39	28.16	31.86	35.85	39.54	40.73	42.92	44.94	45.71	44.76	45.6	46.62	46.95	47.56	47.51	47	47.3	47.38
2.5	3.14	5.22	7.81	10.75	13.92	16.94	19.55	22.13	24.9	27.46	28.28	29.81	31.21	31.74	31.08	31.67	32.37	32.6	33.03	32.99	32.64	32.85	32.9
2	2.01	3.34	5	6.88	8.91	10.84	12.51	14.16	15.93	17.57	18.1	19.08	19.97	20.32	19.89	20.27	20.72	20.87	21.14	21.12	20.89	21.02	21.06
1.5	1.13	1.88	2.81	3.87	5.01	6.1	7.04	7.97	8.96	9.88	10.18	10.73	11.24	11.43	11.19	11.4	11.65	11.74	11.89	11.88	11.75	11.82	11.85
1	0.5	0.83	1.25	1.72	2.23	2.71	3.13	3.54	3.98	4.39	4.53	4.77	4.99	5.08	4.97	5.07	5.18	5.22	5.28	5.28	5.22	5.26	5.26
0.5	0.13	0.21	0.31	0.43	0.56	0.68	0.78	0.89	1	1.1	1.13	1.19	1.25	1.27	1.24	1.27	1.3	1.3	1.32	1.32	1.31	1.31	1.32

Fig. 7. Absorbed power performance (kW) matrix of the considered point absorber WEC based on 3600 s time-domain simulation.

array configurations and system parameters, including the geometric layout and PTO system, are detailed.

2.1. Study areas

The study areas were selected in a way that they have been affected by climatic changes in recent years. Table 1 shows the details of considered areas to study the power performance of case study WEC arrays. Moreover, their geographical locations on the map are illustrated in Fig. 1. These areas are spread across four major ocean regions: Western Tropical Pacific, Southwest Indian Ocean, North Pacific, and South Atlantic. The chosen regions are selected based on their diverse wave energy characteristics, spanning multiple ocean basins with distinct meteorological and oceanographic conditions. These regions represent a range of wave climates, including high-energy environments and lower-energy tropical regions. The inclusion of different climatic regimes, such as monsoonal influences in the Southwest Indian Ocean and the effects of strong westerly winds in the South Atlantic, ensures that the study captures a wide spectrum of wave energy variations driven by long-term climate trends. Furthermore, these locations are strategically selected to cover both developed and emerging wave energy resource regions that contribute to the global understanding of the impacts of climate change on WEC performance. The availability of long-term, high-resolution wave data from ERA5 for these regions allows for a robust statistical assessment of wave energy trends. This diverse selection enhances the representativeness of the study and strengthens its contribution to the field of wave energy converter performance analysis under climate change scenarios.

2.2. Wave climate dataset

In this study, the considered areas' wave climate data are collected from the ERA5 reanalysis dataset [42] to analyze the long-term effects of climate change on studied WEC arrays. The ERA5 is produced by the ECMWF. It is the fifth-generation reanalysis of the global climate and weather, providing high-resolution data over the past eight decades from 1940 onwards. ERA5 provides data from 1979 onward, while earlier periods are based on reanalysis estimates. The dataset offers hourly estimates of various atmospheric, land, and oceanic parameters on a global scale, with a spatial resolution of 0.5° × 0.5° for ocean wave parameters. Here, yearly wave parameters including Significant height of combined wind waves and swell (H_s), Peak wave period (T_p), and Mean wave direction (β) are extracted for the selected points (Table 1) from 1940 to 2023. These data provide insights into the long-term variability and trends in wave conditions, which are critical for assessing how climate change might impact the energy potential of

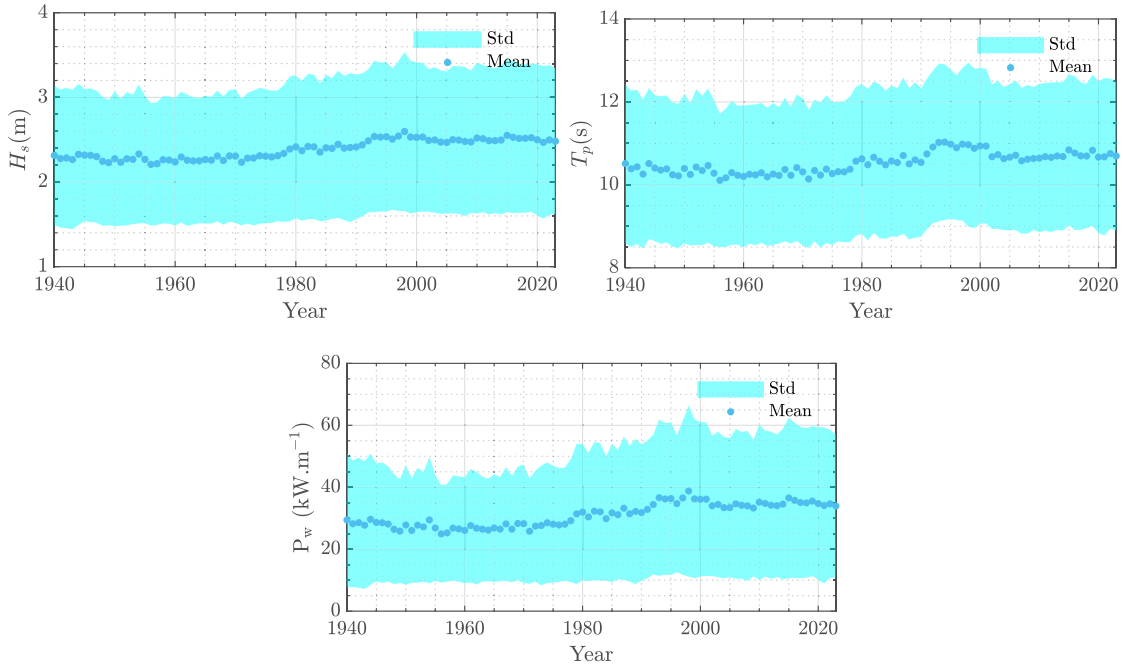

Fig. 8. The overall yearly mean±std of H_s, T_p, P_w of all spatially discretized points of the world oceans from 1940 to 2023.

Table 1
Considered areas to study the power performance of case study WEC arrays.

Region	Location	Coordinates	Water depth (m)
Western Tropical Pacific	Soghonara Island, Solomon Islands	9.0° S, 160.0° E	100
	Port Moresby, Papua New Guinea	9.5° S, 147.0° E	200
Southwest Indian Ocean	Victoria, Seychelles	5.0° S, 56.0° E	115
	Vohemar, Madagascar	13.0° S, 50.0° E	250
North Pacific	Huntington Beach, California	33.5° N, 118.0° W	250
	Vancouver Island, Canada	48.5° N, 125.5° W	100
South Atlantic	Cape Town, South Africa	33.5° S, 18.0° E	200
	Rio de Janeiro, Brazil	23.0° S, 43.0° W	100

WECs. Fig. 2 shows the overall hourly mean of collected data for the world's H_s and T_p from 1940 to 2023. Moreover, the overall globe hourly mean of H_s values for different seasons is illustrated in Fig. 3. According to these figures, the Southern Ocean is the most active region globally in terms of both wave height and period.

2.3. Studied WEC array layouts

In this study, four distinct types of single-body heaving point absorber homogeneous WEC arrays are considered. The point absorber WECs are a widely used technology due to their ability to harness energy from a wide range of wave directions and frequencies [43]. These WECs operate by utilizing the vertical motion of the waves (heaving) to generate power, making them well-suited for a variety of wave climates [44]. The arrays are designed to be homogeneous, which means that each unit within the array is identical in terms of size, shape, and power conversion capacity. This uniformity ensures consistent performance across the array and simplifies the modeling and comparison of power output across different layouts. This approach provides a robust foundation for comparing the energy yield and resilience of different WEC array configurations in diverse wave climates.

The WEC used in this study consists of a solid combined structure with a hemispherical base and a cylindrical top. The hemispherical bottom is designed to provide hydrodynamic stability, while the cylindrical upper section enhances energy absorption from the vertical heaving motion of the waves. This hybrid design maximizes the efficiency of the point absorber by allowing it to respond effectively to a wide range of wave conditions. The hemisphere has a radius of 4 m. The cylindrical section has a height of 6 m with a draught of 6 m. Each WEC in the array is equipped with a linear Power Take-Off (PTO) system with no stiffness and damping 1.2×10^6 N m^{-1} s.

For the analysis, four different WEC array layouts (Fig. 4) are considered to evaluate their performance and energy capture efficiency. The first one is a triangle layout with equal spacing of 100 m between each unit. the triangular layout may enhance constructive wave interactions, which leads to improved power absorption in certain conditions. The second one is a square layout with a spacing of 100 m between each unit. The WECs are placed at the corners of the square. The square layout with the uniform spacing can contribute to more stable energy extraction across varying wave conditions. The third one is a rectangular layout with a WEC in the Middle. This array consists of WECs placed at the corners of a rectangle, with an additional WEC located at the center. The length and width of the rectangle are 150 and 100 m, respectively. This layout is designed for areas with directional wave energy, where wave fronts may interact favorably with the central WEC. The last one is a pentagon layout where the WECs are arranged at the vertices of a regular pentagon. The side length of the pentagon layout is considered to be 100 m. The pentagon layout improves the overall structural stability and performance which results in more reliable long-term performance..

3. WEC array equation of motion

The linear potential flow theory is applied to model the interaction between waves and WEC structures. In this approach, the fluid is considered to be inviscid (lacking viscosity), incompressible (constant density), and irrotational (no vorticity). This simplification significantly reduces computational complexity while retaining accuracy for many practical applications [45]. The general form of the equation of motion for a WEC array with N devices in the heave direction is given by [43,46]:

$$\mathbf{M}\ddot{\mathbf{z}}(t) + \int_0^t K_r(t-\tau)\dot{\mathbf{z}}(\tau)\mathrm{d}\tau + \mathbf{C}\dot{\mathbf{z}}(t) + \mathbf{K}\mathbf{z}(t) = \mathbf{F}_{\mathrm{ex}}(t) + \mathbf{F}_{\mathrm{PTO}}(t) \tag{1}$$

where $\mathbf{z}(t) \in \mathbb{R}^N$ is the displacement vector of the heaving WECs. $\dot{\mathbf{z}}(t) \in \mathbb{R}^N$ and $\ddot{\mathbf{z}}(t) \in \mathbb{R}^N$ are the velocity and acceleration vectors of the WECs, respectively. $\mathbf{M} \in \mathbb{R}^{N\times N}$ is the mass matrix of the WEC array, which includes the mass and added mass of each WEC device. $\mathbf{C} \in \mathbb{R}^{N\times N}$ is the damping matrix. $\mathbf{K} \in \mathbb{R}^{N\times N}$ is the stiffness matrix, representing the hydrostatic restoring forces acting on the WECs. The stiffness matrix helps to bring the WECs back to equilibrium after being displaced by waves. $\mathbf{F}_{\mathrm{ex}}(t) \in \mathbb{R}^N$ represents the hydrodynamic excitation force acting on each WEC, induced by the incident waves. $\mathbf{F}_{\mathrm{PTO}}(t) \in \mathbb{R}^N$ is the force exerted by the PTO system on each WEC. K_r is the radiation impulse response function (IRF):

$$K_r(t) = \frac{2}{\pi}\int_0^\infty B_{rd}(\omega)\cos(\omega t)\mathrm{d}\omega \tag{2}$$

where ω and $B_{rd}(\omega)$ are the frequency, and frequency-dependented radiation damping coefficient.

The external force F_{ext} is calculated by convolving the wave elevation $\eta(t)$ with the non-causal excitation IRF $K_{\mathrm{ex}}(t)$ [47]:

$$F_{\mathrm{ex}}(t) = \int_{-\infty}^{\infty} K_{\mathrm{ex}}(t-\tau)\,\eta(\tau)\,\mathrm{d}\tau \tag{3}$$

where

$$K_{\mathrm{ex}}(t) = \frac{1}{2\pi}\int_{-\infty}^{\infty} X(\omega,\beta)\,e^{i\omega t}\mathrm{d}\omega \tag{4}$$

here, the incident wave direction is denoted by β, and $X(\cdot,\cdot)$ represents the magnitude of the excitation force.

3.1. WEC array power performance metrics

The performance of the considered WEC arrays is evaluated based on three key metrics that quantify their efficiency in capturing wave energy under various sea states. The following performance criteria are considered in this study:

3.1.1. Average power output

The average power output is calculated as the mean power absorbed by the WEC array over a specified period:

$$P_{\mathrm{avg}} = \frac{1}{T}\int_0^T P_{\mathrm{abs}}(t)\,dt \tag{5}$$

where $P_{\mathrm{abs}}(t)$ is the total instantaneous absorbed power at time t, and T is the time period over which the power is averaged.

3.1.2. Capture width ratio (CWR)

The CWR is a commonly used dimensionless metric to assess the efficiency of a WEC in converting available wave energy into useful power. A higher CWR indicates better performance. For an array, it can be generalized to reflect the combined performance of multiple WECs. The CWR is defined as:

$$\mathrm{CWR} = \frac{P_{\mathrm{abs}}}{P_{\mathrm{wave}}\cdot L_{\mathrm{array}}} \tag{6}$$

where P_{abs} is the total power absorbed by the WEC array, P_{wave} is the incident wave power per meter of the wave front, and L_{array} is the effective length of the array, representing the span of the WECs along the wave front.

3.1.3. Array interaction factor (q-factor)

The q-factor quantifies the hydrodynamic interactions between WECs in an array. It measures the extent to which adjacent WECs influence each other's power absorption, considering both constructive and destructive wave interference:

$$\mathrm{q} = \frac{P_{\mathrm{abs}}}{n\cdot P_{\mathrm{single}}} \tag{7}$$

where P_{abs} is the total power absorbed by the WEC array, P_{single} is the power absorbed by a single WEC in isolation, and n is the number of WECs in the array. A q-factor value greater than 1 indicates constructive interference, while a value less than 1 suggests destructive interference between the WECs.

4. Results

4.1. WEC array modeling

This research employs linear potential flow theory based Ansys Aqwa software to model the hydrodynamic forces induced by waves on the WEC array structure within the frequency domain. Initially, a frequency domain analysis is performed to determine the hydrodynamic coefficients, including added mass, radiation damping, and wave excitation forces. These coefficients are subsequently integrated into the time-domain equation of motion to model the dynamic response to varying wave conditions. The global coordinate system originates at the mean free surface, where the Z-axis points upwards. Wave direction is defined by the angle between the wave propagation path and the positive X-axis, measured counterclockwise. The setup parameters for the frequency domain response analysis are as follows: The setup parameters for the frequency domain response analysis are as follows: Gravitational acceleration is specified as 9.806 m s^{-2}. The water density is set to 1025 kg m^{-3}. Wave directions span from −180 to 180 degrees, discretized into 7 steps. The frequency range under consideration extends from 0.1 to 3.5 rad s^{-1}, discretized into 50 steps. Each WEC body mesh size is set to 0.40 m. Viscous effects are not considered. Moreover, the hydrodynamic interaction between WECs is considered in the modeling, which allows for a more accurate simulation of how the devices influence each other's hydrodynamic parameters. Figs. 5 and 6 depict the added mass and radiation damping coefficients in the heave direction for the upper right corner WEC of Layout 2 (Section 2.3) and its interaction with other WECs in the layout. These figures illustrate the WEC's hydrodynamic response in the frequency domain, accounting for both the direct effects of incident waves and the interactions with other WECs in the array. It should be noted that all figures cannot be presented here due to page number limitations. Therefore, some figures are presented selectively.

Time domain modeling of the WEC array involves simulating the dynamic response of the system under wave conditions obtained from considered locations of the studied areas (Section 2.1). Here, the JONSWAP wave spectrum is used to generate the wave elevation time series based on the studied significant wave height and peak wave period. The simulation time is set to 3600 s with time step 0.1 s for each studied sea state. Fig. 7 shows the absorbed power performance matrix of the considered single-body WEC based on 3600 s time-domain simulation. The values in the matrix cells represent the average absorbed power P_{avg} time series. The power matrix provides a detailed relationship between the sea state parameters and the corresponding output power of the WEC.

4.2. Sea states analysis of the world

This subsection presents the global sea state analysis from 1940 to 2023 by calculating the overall yearly mean of all spatial discretized points of the world oceans (Fig. 8). The analysis highlights changes in wave energy potential across various locations worldwide. According

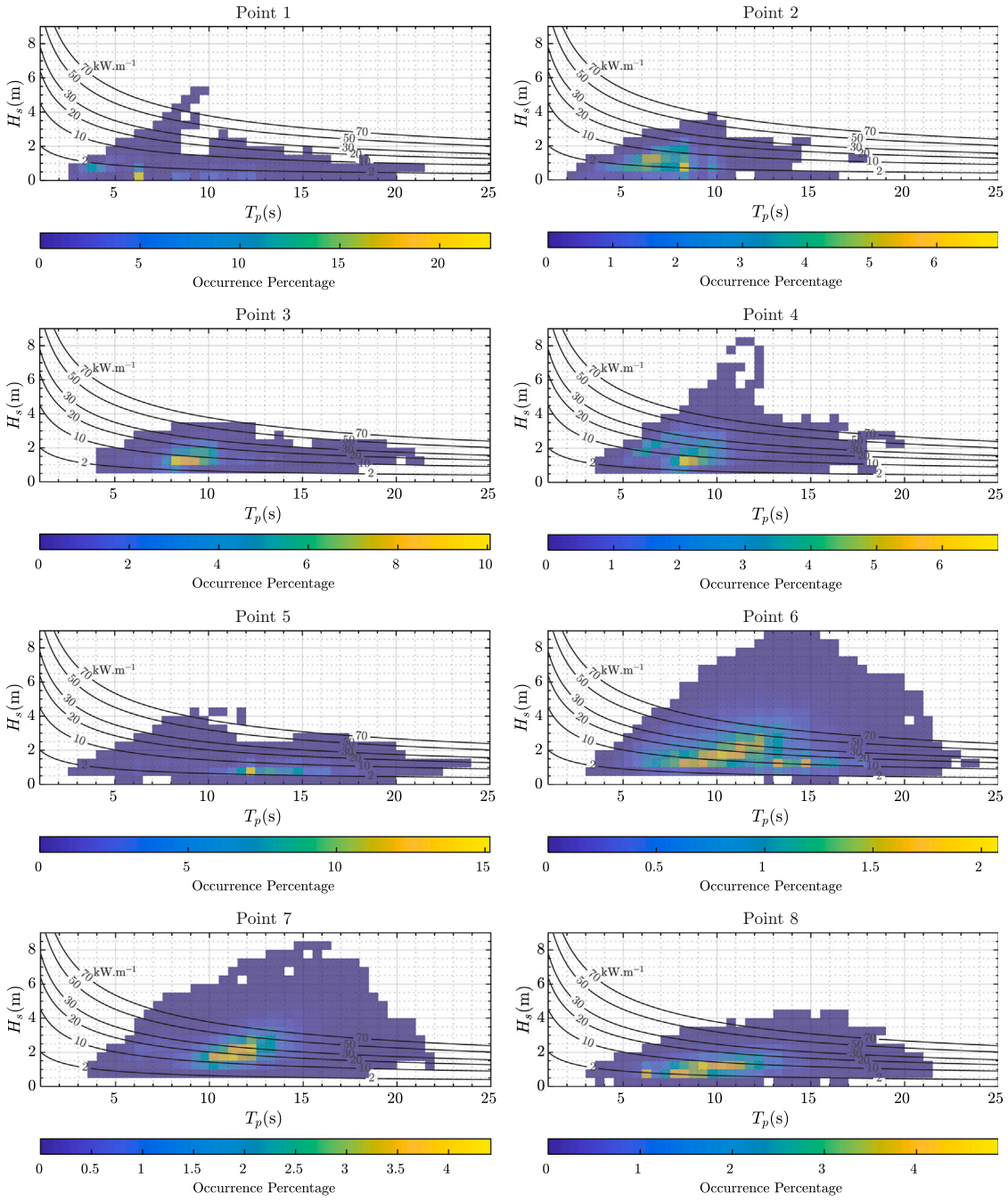

Fig. 9. The sea state bivariate distribution of the studied locations based on ERA5 hourly data from 1940 to 2023.

to this figure, The overall points yearly mean H_s values from 1940 to around 1980 appear to fluctuate within a narrow range (2.21 to 2.31 m), showing general stability with small yearly variations. There are slight dips and peaks but no significant trends, suggesting relatively consistent wave conditions over this period. Around 1980, the values started to rise slightly from 2.30 m to around 2.42 m by the year 2000. This period shows a general upward trend with intermittent variations which indicates an increase in wave energy. After the year 2000, the H_s continues to rise steadily, reaching values as high as 2.54 m by around 2023. The steep rise in H_s during the last 20 years is notable. This trend might be related to increased global oceanic activity, potentially influenced by climate change, which intensifies storm events and wind patterns contributing to larger wave heights. This overall trend of rising H_s suggests a general increase in ocean wave energy and subsequently the performance of wave energy devices. Moreover, the standard deviation (std) of H_s for the studied period (1940–2023) fluctuates between 0.72 m and 0.94 m. There is a general trend of increasing variability in H_s over time, as observed with higher std values in the later years. This increasing trend in H_s variability might indicate growing instability in sea states across the globe.

The T_p values for the years 1940–2023 show a relatively stable trend, with values fluctuating between 10.11 and 11.03 s. Early years exhibit more moderate values, around 10.2–10.4 s, with slight dips and rises over time. Notably, there is a gradual increase in T_p during the last few decades which indicates longer wave periods in recent years. This suggests an overall increase in wave energy transport potential as longer wave periods are often associated with more powerful sea states. However, variability of T_p remains minimal which shows consistent periods over the long term. The analysis of ocean wave power from 1940 to 2023 reveals a clear upward trend. In the early years, wave

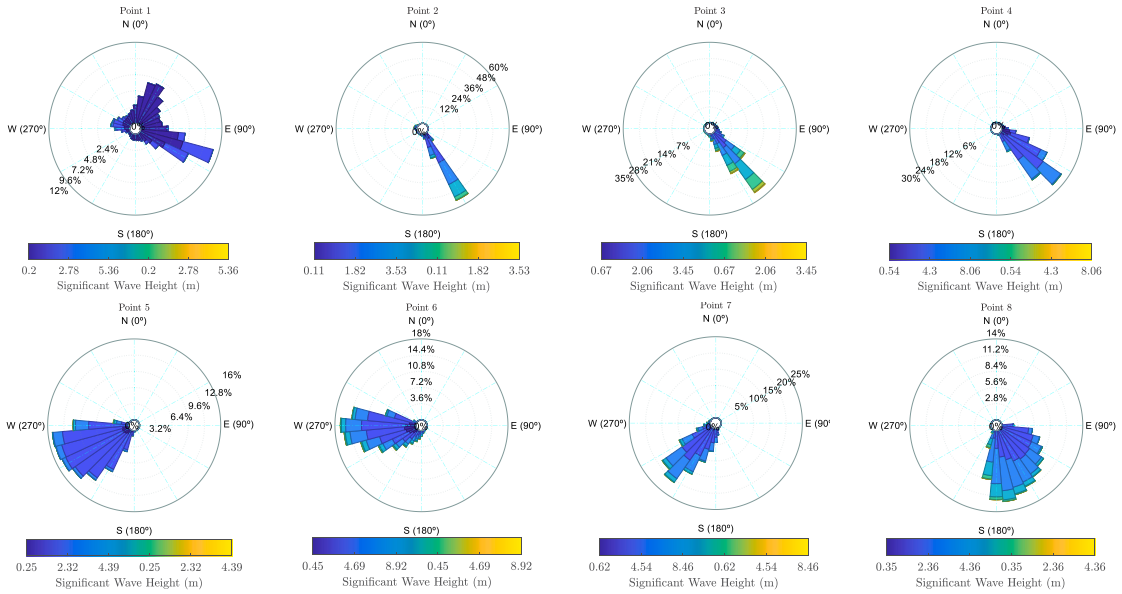

Fig. 10. The wave roses of the studied locations based on ERA5 hourly data from 1940 to 2023.

power ranged from 24.94 to around 29.65 kW m^{-1}, with occasional fluctuations. From the 1970s onwards, wave power begins to steadily increase in recent years. This upward trend, especially prominent in the last few decades, suggests that ocean conditions are becoming more energetic potentially due to increasing storm intensities and climate change effects. Despite some variability, the overall increase indicates a more powerful wave climate globally with significant implications for wave energy harvesting.

4.3. Sea states analysis of the studied points

The sea state analysis provides insights into the wave climate characteristics at the studied locations, which significantly influence the power performance of WECs. For each selected point, wave parameters are analyzed using the hourly resolution ERA5 reanalysis data from 1940 to 2023. Sea states are categorized based on wave heights and wave peak periods, and further separated into different seasonal and monthly intervals to capture variability throughout the year.

Table 2 presents the statistical measures of overall hourly data collected for all studied locations. Moreover, the bivariate distribution of sea state matrices of all studied locations based on H_s and T_p is illustrated in Fig. 9. The contours in this figure are the wave power per unit of wave-crest length (kW m^{-1}). According to this figure, a diverse range of sea states across different points can be seen. A majority of the sea states are concentrated around lower wave heights and shorter periods. In general, the data shows a tendency towards moderate sea states, while extreme events (very high H_s and long T_p) are rare, as reflected by the low percentages in those bins. The most frequent sea state in the bivariate distribution matrix corresponds to the bin with the highest percentage value. Based on the matrix provided for Point 1, the bin with H_s = [0 0.5] m and T_p = [6 6.5] s has the highest occurrence percentage of 22.5%. Therefore, Point 1 experiences more frequent, lower-energy sea states, suitable for smaller WEC designs. Points 6 and 7 show a broader range of sea states. Point 6 has relatively low occurrence percentages (peaking at 2%) but includes a broader distribution across higher energy states. The wave power contours indicate higher power values at Points 6 and 7 due to the higher significant wave heights and longer periods. Points 2 and 3 generally show lower wave power values with a mixture of short and long period waves.

The wave roses of the studied locations are presented in Fig. 10 [48]. Each plot shows the direction from which waves are coming, with percentages representing the occurrence frequency of waves from each direction. The units are in true degrees. It means the direction relative to the geographic North Pole. This shows the origin of the waves: 0 degrees means they come from the north, and 90 degrees means they come from the east. According to this figure, the directions vary across the different points, with some locations experiencing waves from more concentrated directions (like Points 2 and 3), while others see waves from a wider spread (like Points 1, 5, and 8). Point 2 experiences the most concentrated directional pattern, which is ideal for directional wave energy devices designed to capture waves from a fixed direction. Points 1 to 4 show waves predominantly from the southeast. Point 1 exhibits a greater distribution of wave directions, predominantly from the southeast (about 12%) or northeast (about 4.8%). For Points 5 to 7, waves predominantly come from the west and southwest, with a peak occurrence of around 16%, 18%, and 25%, respectively. Waves predominantly arrive from the south for Point 8. The differences in wave directionality and significant wave heights across these points suggest that each location would benefit from tailored WEC designs optimized for its specific wave conditions.

Fig. 11 presents the overall yearly mean±std of H_s for the studied locations from 1940 to 2023. According to this figure, most locations show a general increase in H_s values over time. This increase is consistent with the impacts of climate change, which is expected to intensify wind speeds and wave activity due to warmer sea surface temperatures and changing storm patterns. Point 1 is situated in a region with low wave power, as H_s values hover around 0.5 to 1 m. Points 4, 6, and 7 exhibit higher H_s values, representing regions more exposed to storms or powerful wind fetch, with H_s values consistently between 2.0 to 2.5 m in recent years. Point 2 fluctuates around 1.0 to 1.15 m, with a slight increasing trend. This location likely experiences modest increases in wind energy. Point 3 Shows a consistent increase from around 1.37 m to 1.56 m. Point 8 consistently increases over time, peaking at around 1.36 m from initial values of around 1 m. This situation is also true for Point 7. Moreover, the overall yearly mean±std of T_p for the studied locations is shown in Fig. A.1. This figure suggests that despite fluctuations, the trend does not show significant long-term increases. However, slight fluctuations might still be connected to seasonal variations. Points 1 to 4 tend to have lower overall T_p values which range from around 5 to 10 s. For instance, Point 1 has mean values that vary around 6.4 to 7.8 s which shows slight fluctuations, while Points 2 and 3 follow a similar trend, with Point 3 reaching up to 9.73 s. Points 5 to 8 display higher T_p values,

Table 2
The sea state statistical measures of the studied locations based on ERA5 hourly data from 1940 to 2023.

Data set	Feature	Point number							
		Point 1	Point 2	Point 3	Point 4	Point 5	Point 6	Point 7	Point 8
H_s	Mean	0.56	1.04	1.46	1.82	0.86	2.12	2.23	1.22
	Median	0.48	0.96	1.38	1.74	0.81	1.87	2.11	1.13
	Std	0.25	0.48	0.41	0.64	0.27	0.99	0.73	0.44
	Variance	0.06	0.23	0.17	0.42	0.07	0.99	0.53	0.19
	Min	0.19	0.11	0.66	0.54	0.25	0.44	0.61	0.35
	Max	5.36	3.52	3.44	8.06	4.39	8.92	8.46	4.35
	Range	0.26	0.69	0.62	0.98	0.27	1.3	0.9	0.55
	Skewness	2.42	0.69	0.72	0.58	2.02	1.21	1.12	1.14
	Kurtosis	14.19	3.05	2.96	2.98	11.14	4.76	5.25	4.72
T_p	Mean	7.07	7.18	9.18	8.48	12.91	11.38	11.6	9.96
	Median	6.17	7.28	9.07	8.47	12.87	11.36	11.7	9.88
	Std	2.96	1.47	1.33	1.46	2.52	2.81	1.94	2.19
	Variance	8.78	2.18	1.78	2.14	6.39	7.91	3.77	4.8
	Min	2.56	2.03	4.01	3.69	2.91	3.3	3.67	3.31
	Max	21.1	17.53	21.02	19.54	23.65	23.68	21.94	21.48
	Range	5.14	1.99	1.55	1.81	2.61	4.01	2.28	3.07
	Skewness	0.75	−0.25	0.73	0.3	−0.53	0.12	−0.19	0.28
	Kurtosis	2.79	2.99	5.85	4.14	4.01	2.65	3.88	2.86

especially Points 5 and 6, where T_p mean often exceeds 12 s. These longer-period waves are characteristic of the open ocean regions where storms are more frequent, generating powerful, long-period swells. In general, no dramatic increases are observed over time, indicating that while climate change might be impacting storm behavior, it may not be drastically altering T_p at these locations in the studied period.

Fig. 12 presents the overall yearly mean±std of P_w for the studied locations. Points 1, 2, and 5 show lower overall wave power compared to the others. While there are fluctuations, especially in Point 1, the trend appears to have mild variations. Points 6 and 7 show consistently high wave power values, particularly in more recent years (post-1980s), which could indicate stronger or more frequent storms or larger waves driven by ocean currents and changes in wind patterns due to climate change. There is a general rising trend in wave power in Points 7 and 8. Point 6, in particular, shows some significant variations, with mean values ranging from 19 kW m^{-1} to peaks of 40 kW m^{-1}, especially in recent decades. Similarly, Point 7 exhibits high and increasing wave power values, peaking at 39.29 kW m^{-1} in some years. The data shows increased variability in wave power in many locations, especially after the 1980s. The increase in wave power in certain regions (e.g., Points 6 and 7) may provide enhanced opportunities for wave energy exploitation. However, the increased variability may also pose challenges for the consistent WECs' performance. This suggests a need to optimize WEC designs to handle a wider range of wave conditions efficiently.

The overall seasonal mean boxplot of P_w for the studied locations is illustrated in Fig. 13. According to this figure, winter and summer generally have higher wave power compared to the other seasons, particularly at Points 1 and 4, where the maximum values are notably higher. Points 6 and 7 exhibit the highest P_w during all seasons which indicates potentially more energetic seas. Points 1 and 5 tend to have consistently low wave power throughout all seasons. Some points, such as Point 8, show higher wave power during spring than winter, which may reflect local oceanographic conditions or exposure to different wave systems. Most points exhibit the highest median P_w during the summer season, with Points 6, and 7 displaying larger values. The interquartile range (IQR) is also broader for these points, suggesting more variability and higher energy waves. In general, winter has the lowest median P_w. The red dots represent outliers, or extreme wave power values that fall beyond the whiskers of the boxplots. These dots can be interpreted as individual extreme wave events, storms, or other rare conditions that significantly increased P_w for short periods. Points 4, 6, and 7 have numerous high outliers in all seasons that suggest these locations are subject to extreme wave events throughout the year. The presence of many outliers indicates the importance of accounting for extreme wave events when designing wave energy systems. Moreover, additional results about the seasonal variations of H_s and T_p of the studied locations are provided in Fig. A.2 and Fig. A.3, respectively.

The overall monthly mean boxplot of P_w for the studied locations is illustrated in Fig. 14. Moreover, the overall monthly mean of the H_s and T_p are shown in Fig. A.4 and Fig. A.5, respectively. Based on Fig. 14, in most of locations (except Point 6 and Point 5), wave power is higher during the summer months (June to August) and lower during the winter and autumn months. Point 6 exhibits the highest wave power values, with peak values occurring in the winter months (December to February). Point 1 and Point 5 have relatively lower and more stable wave power values throughout the year, with minor fluctuations. Point 7 maintains relatively high wave power values consistently throughout the year, with a peak in June and a minimum in January. Point 6 has the highest IQR values, peaking at 48.23 kW m^{-1} in December. This indicates a wide range of wave power values and significant variability throughout the year. Point 1 has the lowest IQR values, with the highest being 1.2 kW m^{-1} in February and the lowest being 0.46 kW m^{-1} in May. Point 2, Point 3, Point 4, Point 6, and Point 7 show significant seasonal variations, with higher IQR values during the middle of the year (summer months) and lower values during the beginning and end of the year (winter months). Point 1 and Point 5 have relatively lower and more stable IQR values throughout the year which indicates less variability in wave power.

4.4. Climate change impacts on WECs' power performance

To represent the overall hourly data in the form of annual or seasonal, and capture climate-driven trends in wave characteristics, it is helpful to compute summary statistics and key metrics for each studied point during the considered temporal resolution. The considered measures of the sea states are mean and median which show the central tendency, 10th percentile which indicates calmer wave conditions, and 90th percentile which highlights extreme conditions that are relevant for assessing high wave impacts on WECs. These statistical metrics are calculated for considered WEC array power performance metrics (Section 3.1) of each considered WEC layout (Section 2.3). These measures summarize sea states of considered temporal resolution and give insights into trends and variability driven by climate change.

Fig. 15 presents the yearly absorbed power of considered single-body WEC for the studied locations from 1940 to 2023, obtained by the overall yearly mean of the sea states. The mean absorbed power increases steadily over time for all studied points, suggesting a general upward trend in wave energy. The median follows a similar trend to the mean but shows slightly lower values. It indicates that while the average wave energy is increasing, the distribution might be skewed

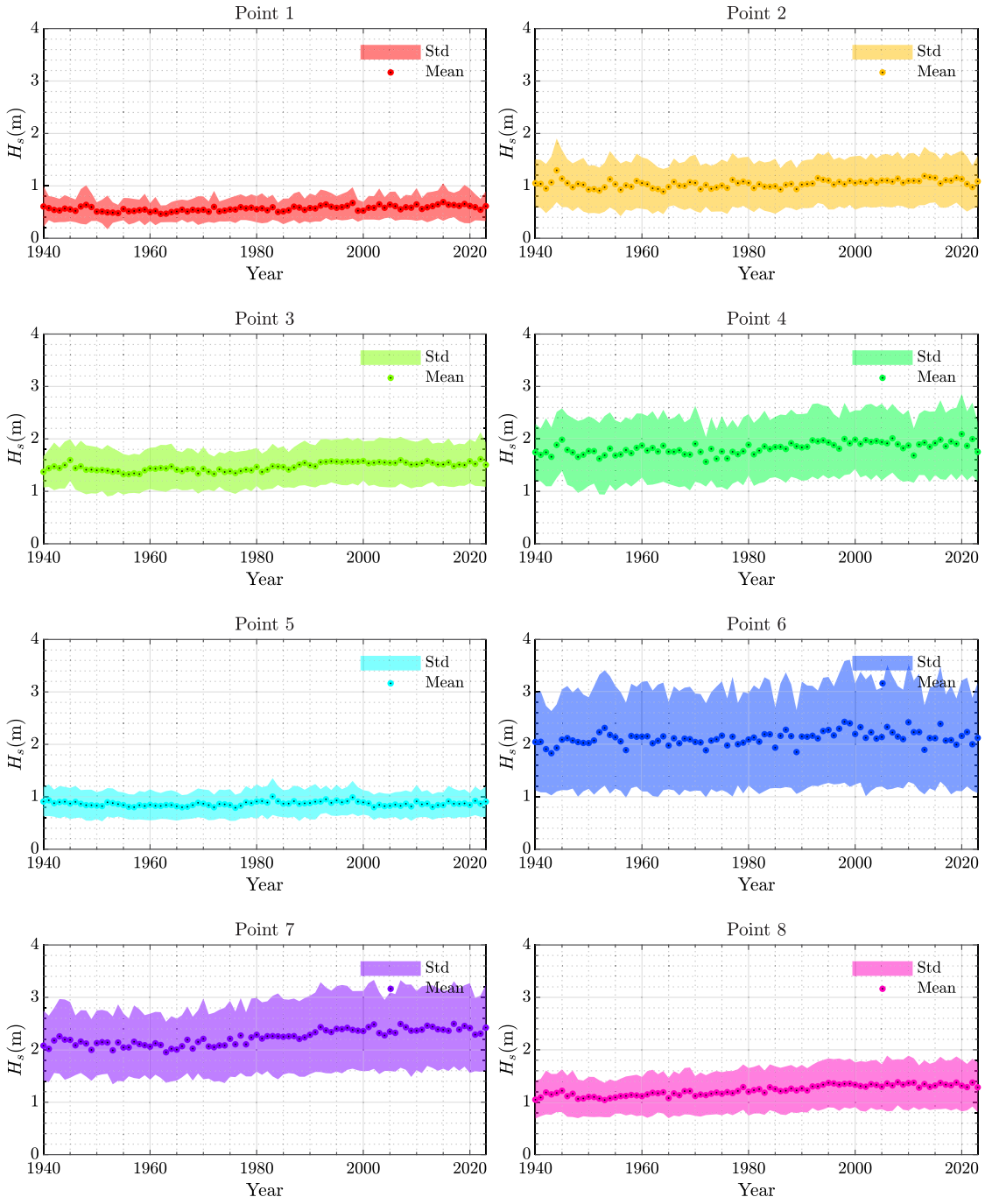

Fig. 11. The overall yearly mean±std of H_s for the studied locations from 1940 to 2023.

by higher extreme values. In general, 90th percentile shows a sharper increase over time, more pronounced than the mean or median. This indicates that the highest waves' power is increasing significantly and suggests more frequent extreme wave events. The 10th percentile also increases over time but at a much slower rate, indicating that the lowest energy waves are relatively stable. These trends suggest a growing disparity in wave power, with high-energy events becoming more frequent and intense while lower energy events remain relatively stable. This has implications for the design and operation of wave energy converters, as they need to be robust enough to handle increasing extreme events while still capturing energy efficiently from waves.

Fig. 16 presents the yearly total absorbed power of considered WEC array layouts for the studied locations from 1940 to 2023, obtained by the overall yearly mean of the sea states. According to this figure, all considered WEC layouts show an upward trend in absorbed power from 1940 to 2023. This suggests improvements in wave energy harvesting technology and possibly increasing wave energy availability over the decades. Layouts 3 and 4 are more efficient, absorbing more power consistently compared to Layouts 1 and 2. The variations in the absorbed power year by year highlight the impact of changing wave conditions. Layout 4 consistently exhibits the highest absorbed power, suggesting it might be the most efficient and effective configuration among the four layouts. The linear trend line for Layout 4 has a steep positive slope, which indicates a considerable increase in total absorbed power over the years. Layout 1 has the lowest absorbed power overall. Its trend

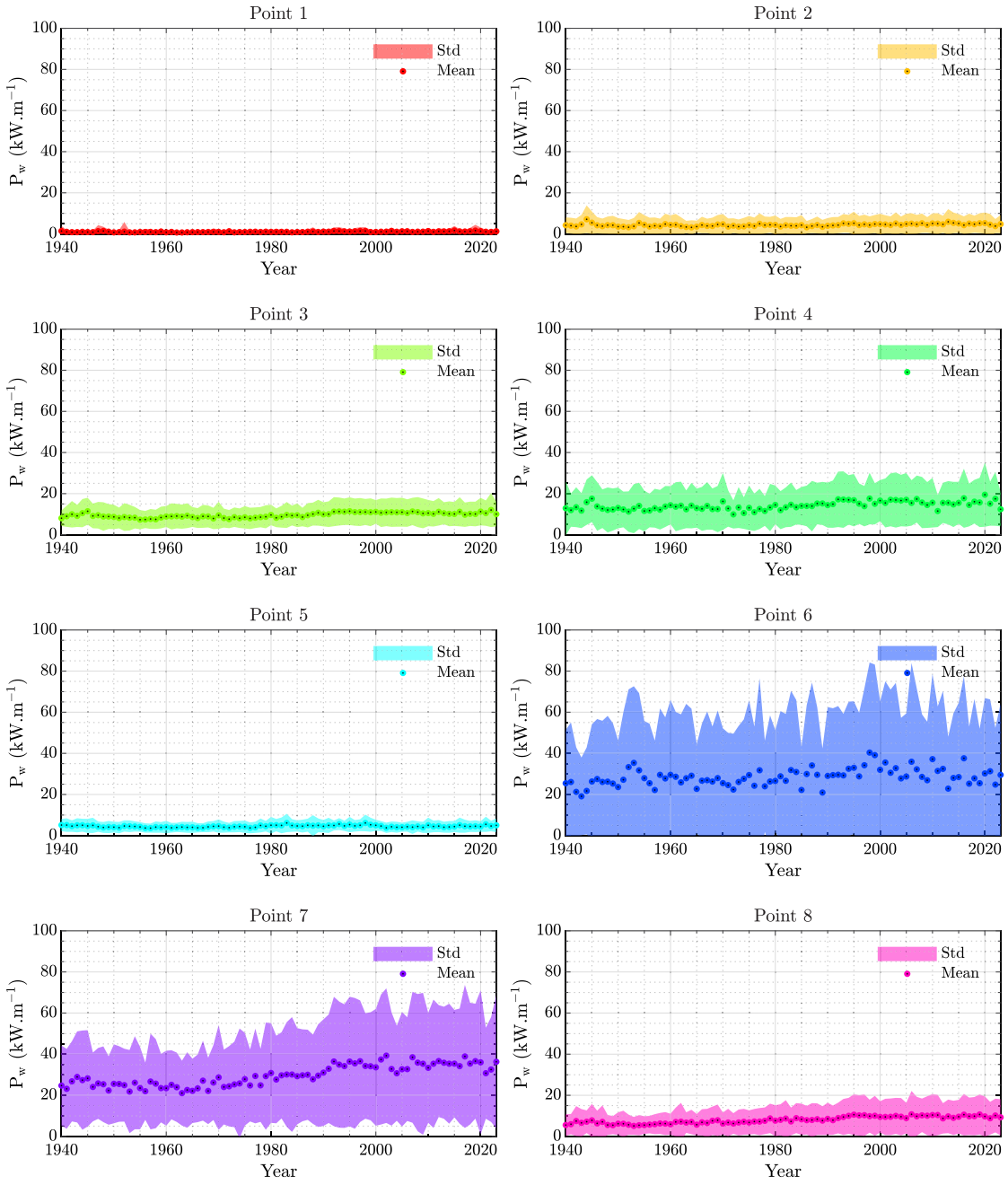

Fig. 12. The overall yearly mean±std of P_w for the studied locations from 1940 to 2023.

line is the least steep, representing the slowest growth rate among the layouts.

For more details of other performance metrics, the yearly capture width ratio and q-factor of these points based on the overall yearly mean of the sea states are shown in Fig. 17 and Fig. 18, respectively. According to these figures, given that the general trend of total absorbed power (P_{avg}) is increasing over the years, but CWR and q-factor do not exhibit the same clear upward trend. P_{wave} is proportional to the square of significant wave height and wave energy period. If the absorbed power does not increase proportionally with the wave power, it could result in a stable or even declining CWR. This might happen if WECs become less efficient under certain wave conditions. CWR reflects the efficiency of the WEC in converting wave energy. If the energy conversion efficiency by the WECs decreases over time (due to degradation or suboptimal wave conditions), this would cause a decline in CWR, even if P_{abs} increases. Different WEC array layouts may respond differently to changes in wave direction. If the wave direction varies over time, certain layouts may capture less energy effectively, reducing the CWR even if P_{abs} is increasing. Here, L is constant, so this parameter would not influence changes in CWR over time.

The q-factor does not exhibit the same increasing trend as P_{wave} based on Fig. 18. This phenomenon can stem from constructive and destructive interference between waves and the WECs in the array. The layout and distance between individual WECs influence how waves propagate through the array. In years where wave conditions align well with the optimal configuration of the array, constructive interference may be more prevalent, resulting in a higher q-factor. In other years, changes in wave conditions could result in more destructive interference between WECs, lowering the q-factor despite an increase in wave energy or absorbed power. Array layout and spacing play a crucial role, as suboptimal configurations lead to energy losses through shadowing and scattering. Additionally, non-linear effects and the mismatch

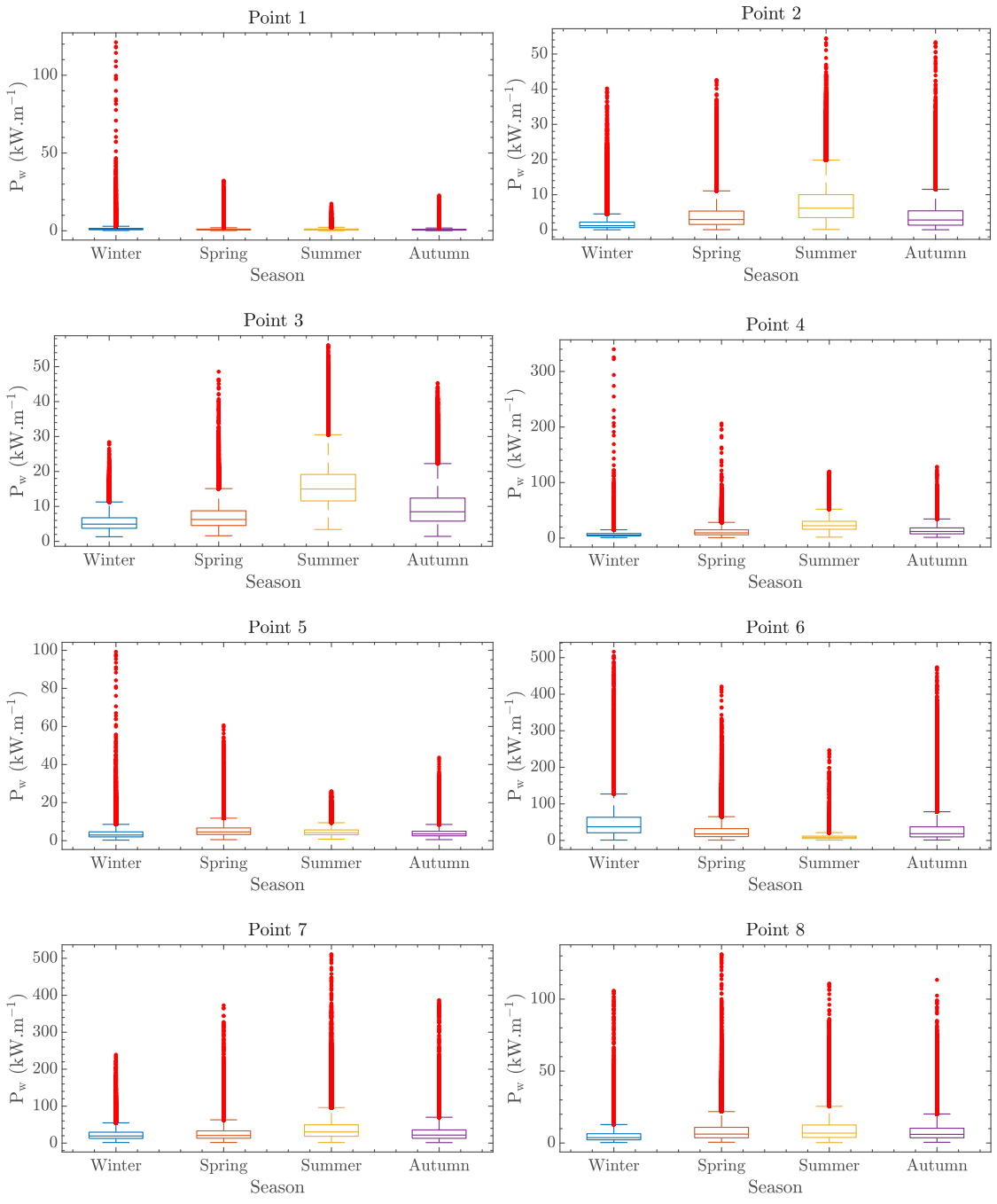

Fig. 13. The overall seasonal mean boxplot of P_w for the studied locations from 1940 to 2023.

between wave frequency and WEC resonance limit efficiency gains. Lastly, temporal variations in wave direction and energy over time cause changes in interference patterns, which can prevent consistent improvements in the q-factor despite the overall rise in wave energy.

In order to summarize the results and avoid providing multiple figures, a summary of the overall trend of the considered time series is presented in Tables 3 to 5 based on Mann–Kendall trend test [49,50]. It is a non-parametric test and robust to outliers (either increasing or decreasing) that identifies monotonic trends in time-series data which is useful for analyzing long-term trends in WECs' power performance data. For wave condition data which often contains variability, seasonality, and possibly outliers (e.g., from extreme weather events), robust methods that can handle non-linear trends and are less sensitive to outliers are generally more suitable. The test provides both the direction and significance of the trend. A positive Kendall's Tau coefficient indicates an upward trend, while a negative value indicates a downward trend.

Table 3 summarizes the yearly total absorbed power trends for different WEC array layouts across eight study points. Overall, most locations show positive Tau values across all layouts which implies that the general trend in absorbed power has been upward over the study period. However, the magnitude of these trends varies by point and layout. Points 7 and 8 generally show the highest positive Tau values across layouts, indicating that these locations have experienced the most significant upward trends in power absorption. Conversely, Point 5 displays notably lower or even negative Tau values, particularly for the 10th percentile in some layouts. Layouts 1 and 2 tend to have higher Tau values overall.

According to Table 4, tau coefficients indicate mixed trends across different WEC array layouts and points. While some layouts and points

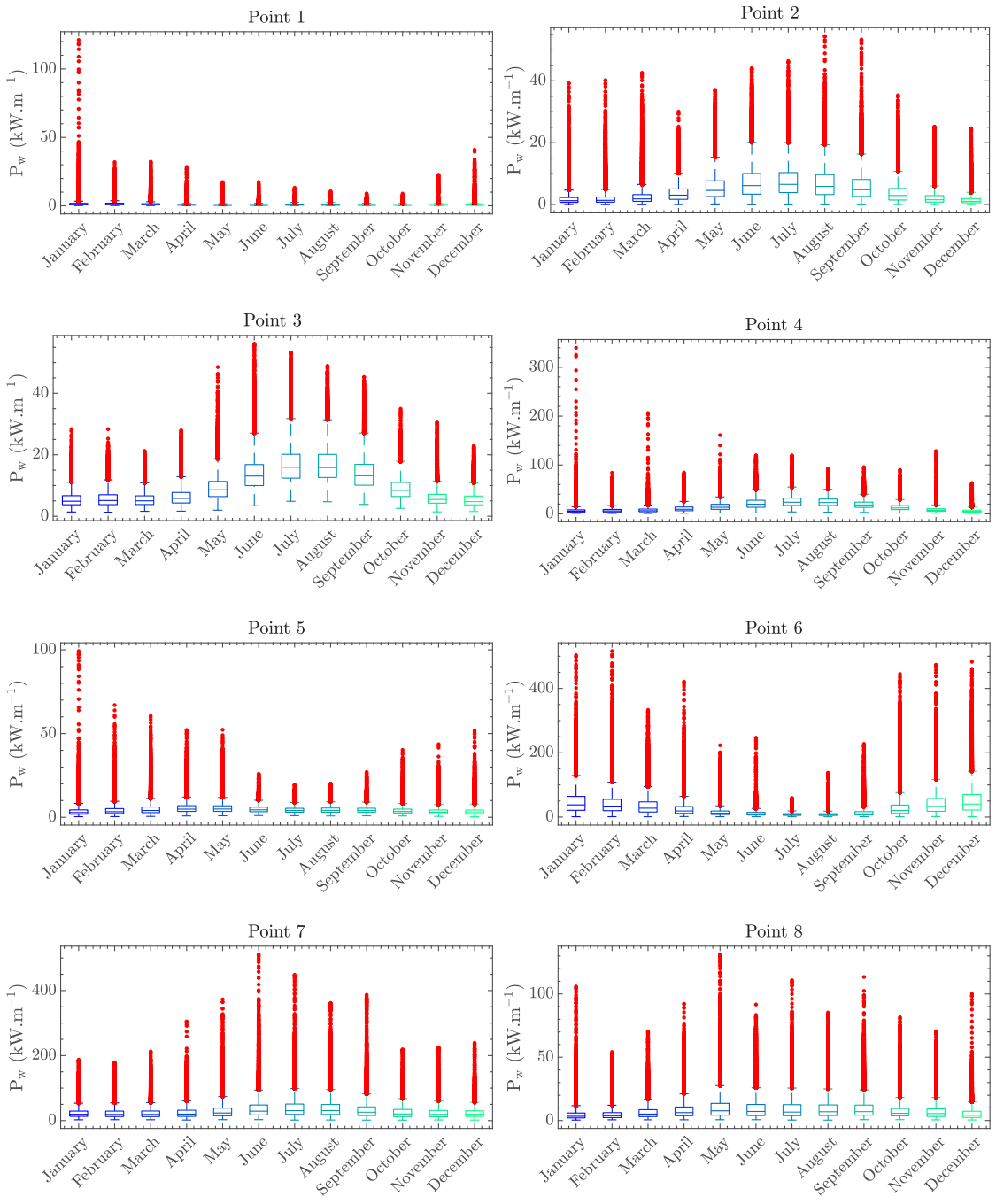

Fig. 14. The overall monthly mean boxplot of P_w for the studied locations from 1940 to 2023.

show increasing trends (positive tau coefficients), others display decreasing trends (negative coefficients). The 10th percentile generally shows positive coefficients, suggesting an increasing trend for lower quantiles. In contrast, the 90th percentile often shows negative coefficients, indicating a decreasing trend for higher quantiles. Based on mixed results, it cannot be said that over time, climate change has necessarily caused an increase or decrease in captured wave energy by the WECs. The variability in trends also suggests that site-specific and design-specific factors play crucial roles in the efficiency and effectiveness of WECs. Moreover, the q-factor analysis using the Mann–Kendall Tau coefficients is shown in Table 5. Here also, the results show diverse trends across different layouts and points. While some points and layouts exhibit increasing trends, most show a decline in q-factor, indicating a reduction in efficiency over time. These mixed results underscore the complexity of long-term performance evaluation and the necessity for continuous monitoring and adaptive strategies to optimize WEC performance. Therefore, it can be said that the climate change does not necessarily increase or decrease the q-factor of the array, but it is the WEC layout, body geometric characteristics, and wave climate that will determine the value of this parameter.

The Mann–Kendall Tau coefficients for the seasonal mean of total absorbed power (P_{avg}) across different WEC layouts from 1940 to 2023 are presented in Table 6. The analysis indicates positive trends in most seasons and WEC layouts and points. However, some mixed results in the summer season suggest variability in wave energy conditions. Winter, spring, and autumn show positive coefficients at all layouts and points, indicating an increasing trend in the total absorbed power. In general, the highest trend is related to points 8 and 7 and the

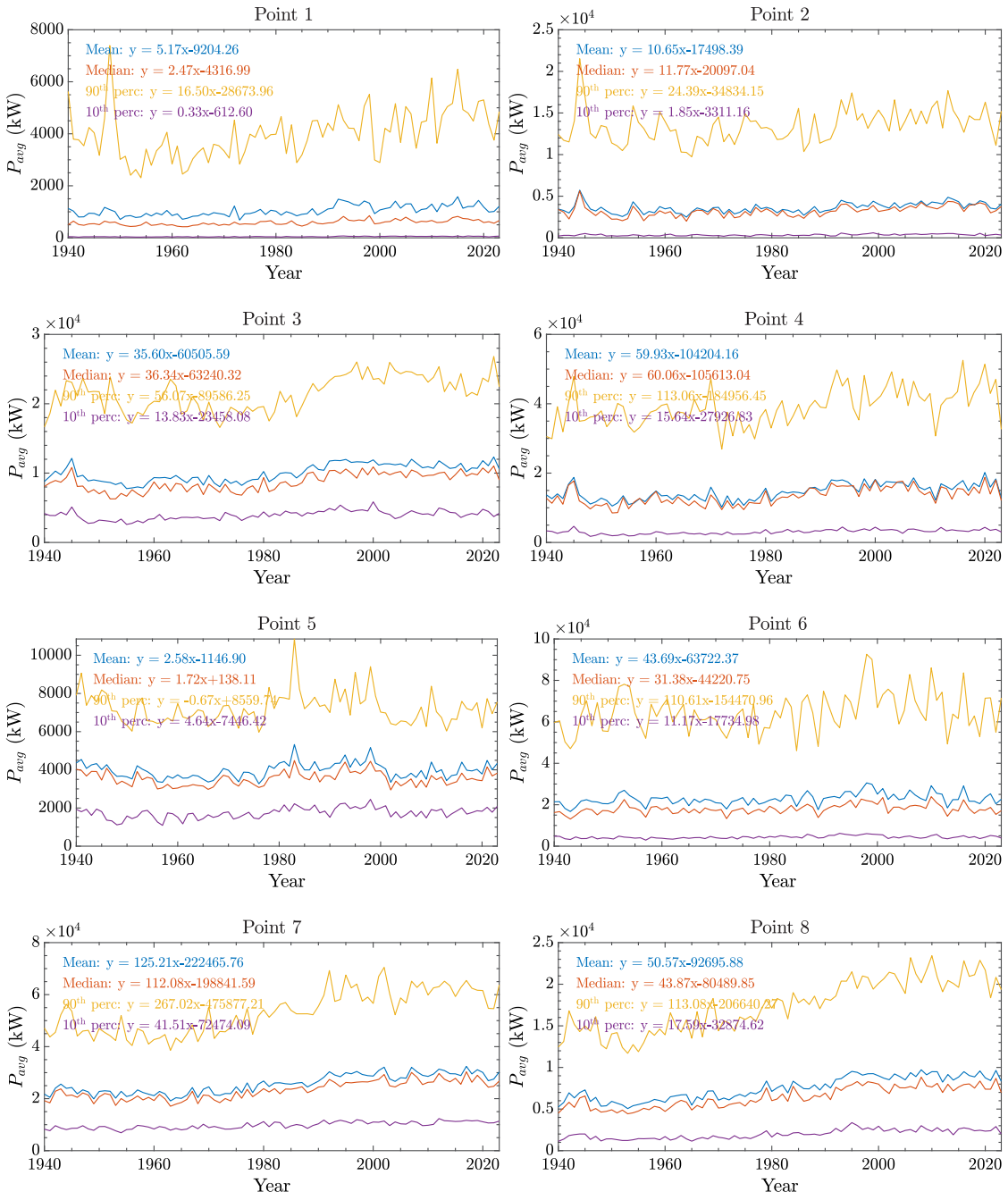

Fig. 15. The yearly absorbed power P_{avg} of considered single-body WEC for the studied locations from 1940 to 2023, obtained by the overall yearly mean of the sea states.

lowest trend is related to points 5 and 2, respectively. On average, the highest positive trend occurs in winter, spring, summer, and autumn, respectively, but this difference is insignificant. The highest trends are observed in Layout 4, 3, 1, and 2, respectively. Moreover for more details, WEC layouts seasonal mean CWR and q-factor Mann–Kendall Tau coefficients are provided in Tables A.1 and A.2.

Given the long-term observed changes in wave climate and their impact on WEC power performance, practical engineering adaptations should be considered to increase the flexibility and efficiency of WECs in a changing ocean environment. One potential approach is to optimize WEC array configurations to better align with anticipated changes in wave height, frequency, and direction, ensuring maximum constructive interference and minimizing energy losses due to destructive interactions. In addition, advances in real-time control strategies could enable adaptive tuning of PTO parameters, which could enable WECs to dynamically respond to fluctuating wave conditions and improve energy capture efficiency. Structural modifications, such as adjustable WEC body geometry or adjustable mooring systems, may also enhance survivability and performance in diverse wave climates. Furthermore, integrating predictive maintenance and reliability assessments could help mitigate the risks associated with increasing wave energy variability and extreme events.

5. Conclusion

This study analyzed the long-term effects of climate change on the power performance of WEC arrays in various global regions using ERA5 hourly wave data from 1940 to 2023. By evaluating different WEC array layouts and examining performance metrics such as the total absorbed power, CWR, and q-factor, the impacts of wave climate changes

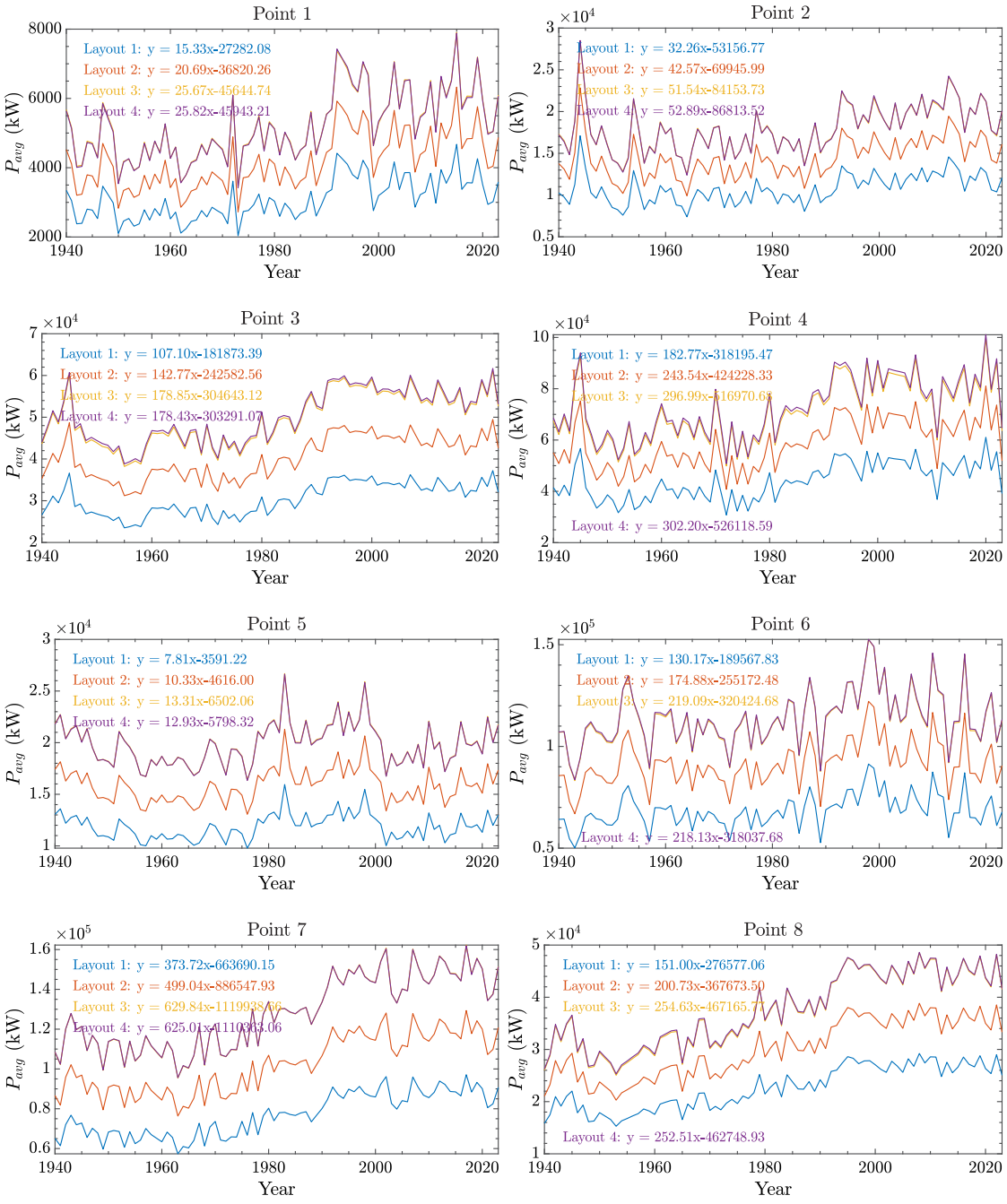

Fig. 16. The yearly total absorbed power P_{avg} of considered WEC array layouts for the studied locations from 1940 to 2023, obtained by the overall yearly mean of the sea states.

were explored on the efficiency and effectiveness of WEC arrays in capturing energy over time. Trends in wave energy availability and WEC power absorption were quantified using different statistical and visualization methods which revealed spatial and temporal variations across different study points. The main findings of this research are as follows:

- **Increasing Trend in Ocean Power:** Global sea state analysis revealed a stable mean significant wave height (H_s) from 1940 to 1980, followed by a gradual rise to 2.42 m by 2000, and a steep increase to 2.54 m by 2023, suggesting increased wave energy likely driven by climate change. The T_p values showed relatively stable trends with slight increases over the decades. Similarly, ocean wave power demonstrated a notable upward trend, especially post-1970s, underscoring more energetic ocean conditions and greater wave energy harvesting potential.
- **Hourly Sea States Analysis of the Studied Points:** The analysis of wave heights (H_s) and peak wave periods (T_p), categorized by season and month, shows a tendency towards moderate sea states at most locations, while extreme conditions are rare. Points 6 and 7 experience higher power values due to higher H_s and longer T_p, while Points 2 and 3 have lower power with mixed wave periods. Directional wave analysis indicates variability across locations, with Points 1 to 4 experiencing southeast waves, Points 5 to 7 predominantly southwest, and Point 8 mainly from the south. Over time, H_s values generally increase across most locations, correlating with climate-induced wind intensification. Although

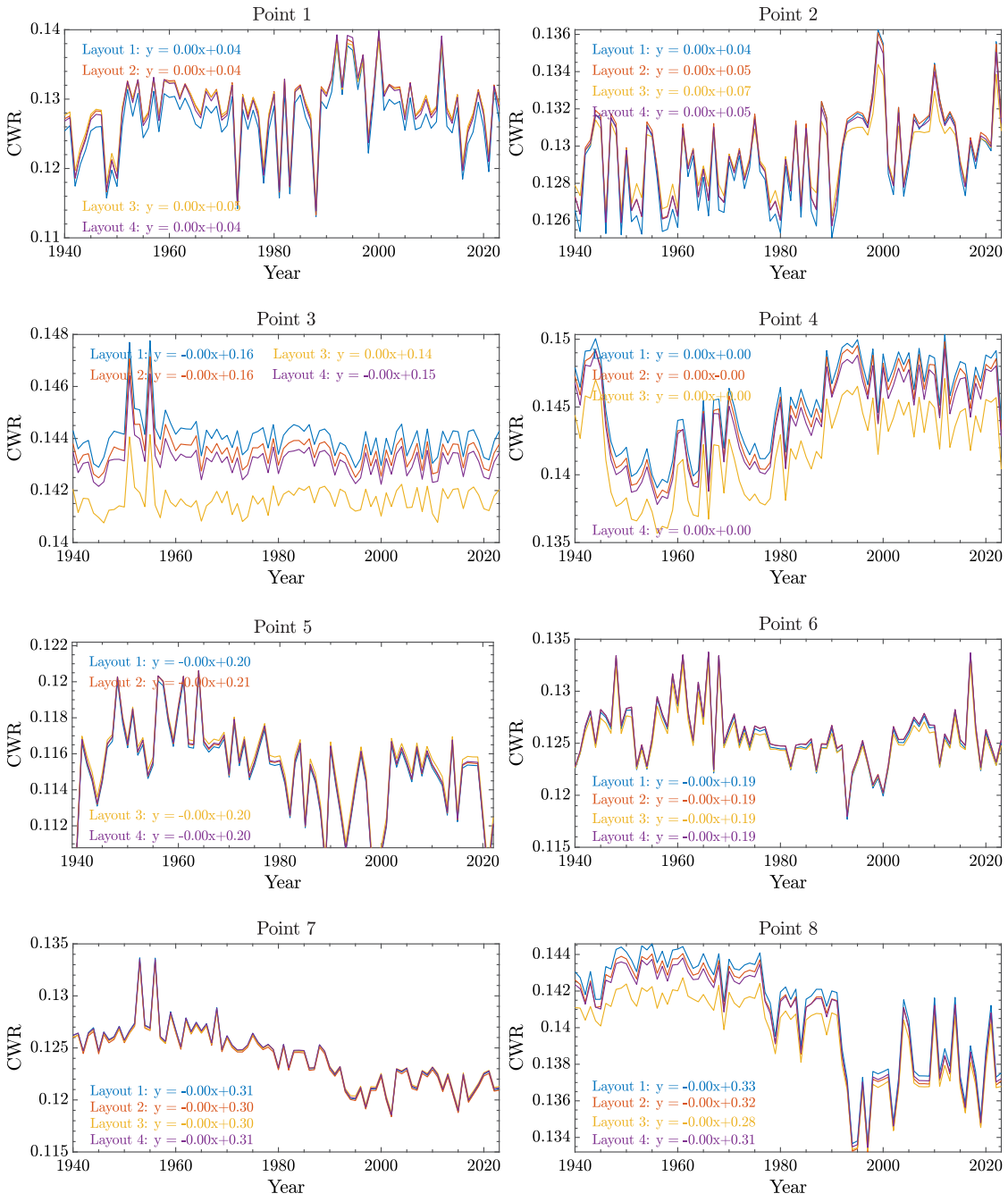

Fig. 17. The yearly capture width ratio of considered WEC array layouts for the studied locations from 1940 to 2023, obtained by the overall yearly mean of the sea states.

T_p values fluctuate, they remain relatively stable, particularly in open ocean regions with longer wave periods at Points 5 and 6. Rising wave power trends, notably at Points 6, 7, and 8, align with potential climate impacts, enhancing wave energy potential but also introducing variability. This increased wave power suggests expanded wave energy opportunities but highlights the importance of adaptable WEC designs to account for fluctuating conditions.

- **Seasonal and Monthly Analysis of Wave Power of the Studied Points:** Winter and summer generally present higher P_w across locations. Seasonally, summer exhibits the highest median wave power, especially for Points 6 and 7, which also have a broader IQR which indicates substantial variability and higher energy waves. Monthly, P_w generally peaks in summer (June-August) and dips in winter, except for Points 6 and 5. Point 6 shows the highest wave power in winter, particularly in December. The variability of P_w is highest at Point 6, peaking at an IQR of 48.23 kW m^{-1} in December, and lowest at Point 1, which has consistently low and stable values. Points 1 and 5's limited variability contrasts with significant seasonal variations and higher mid-year IQR values observed at Points 2, 3, 4, 6, and 7. These trends underscore the influence of seasonal and monthly shifts in wave power.
- **Increasing Trend in Absorbed Power:** Despite variations across locations, the overall trend in absorbed power for most studied WEC arrays was positive. It indicates an increase in wave energy potential over the years due to climate change. This suggests that

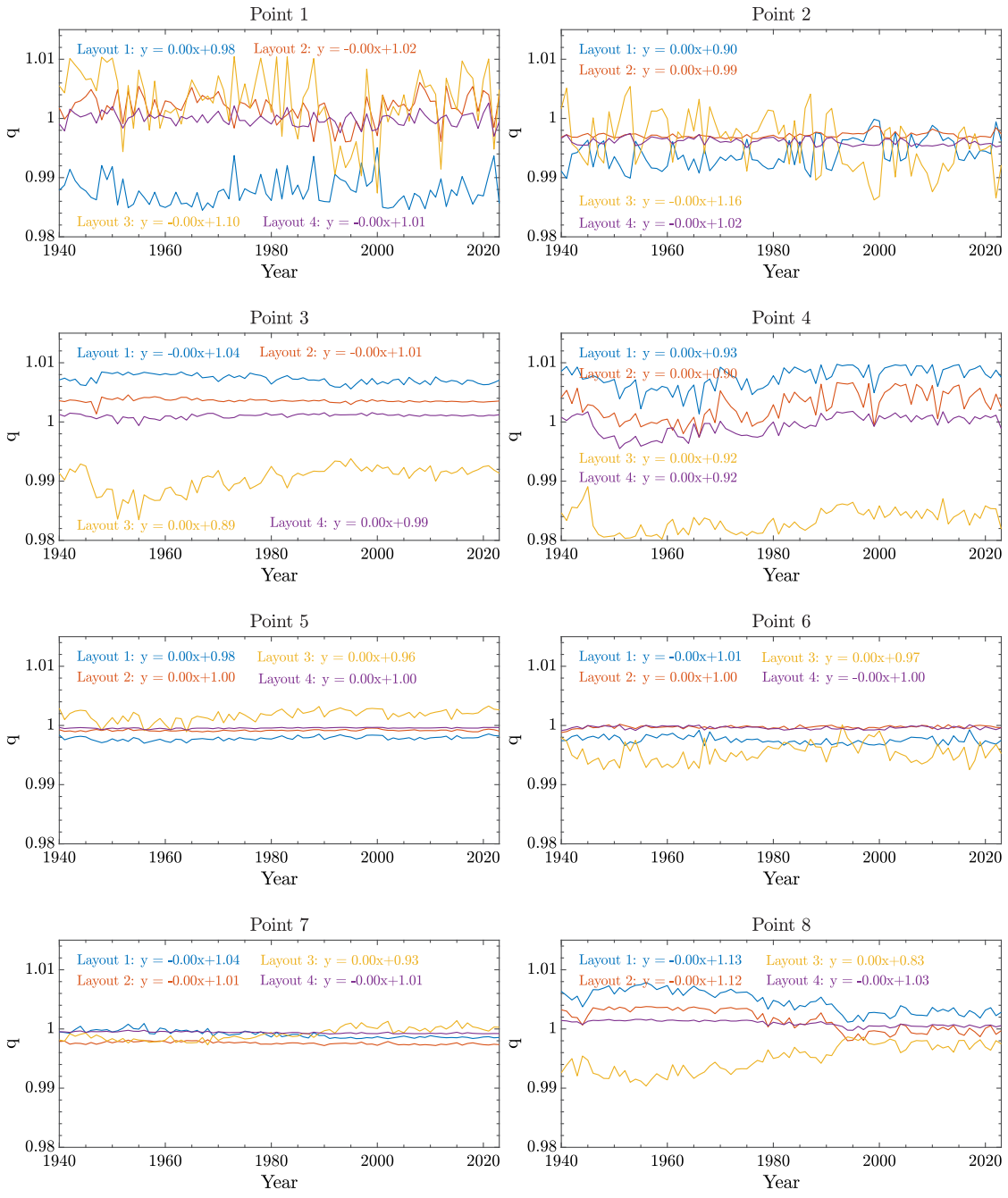

Fig. 18. The yearly q-factor of considered WEC array layouts for the studied locations from 1940 to 2023, obtained by the overall yearly mean of the sea states.

WEC arrays in certain regions can benefit from the changing wave conditions, potentially enhancing their long-term viability as a renewable energy source.

- **Spatial Variability in Trend Magnitude:** Trends in the key sea state metrics — mean, median, 10th, and 90th percentiles — indicate a shift towards more intense wave conditions over time. The mean and median show steady upward trends, suggesting an overall increase in wave energy. However, the 90th percentile, which captures extreme wave conditions, shows a sharper increase, implying a rise in both the frequency and intensity of high-energy wave events. The relatively stable 10th percentile values suggest that calmer wave conditions remain less affected by climate change. Yearly absorbed power for various WEC array layouts further reflects this trend, with each layout showing a positive trend in power absorption over the study period. Layouts 3 and 4 demonstrate the highest efficiency, consistently capturing more power compared to Layouts 1 and 2, with Layout 4 displaying the steepest upward trend.
- **Complexity in CWR and q-Factor Trends:** Although the absorbed power generally increased, the trends in CWR and q-factor were not consistently upward. This complexity can be attributed to wave-structure interactions, including constructive and destructive interference, which vary based on wave direction, frequency, and the specific layout of WEC arrays. In some cases, constructive interactions were insufficient to counterbalance the impacts of destructive wave interactions which led to stable or

Table 3
WEC layouts yearly total absorbed power (P_{avg}) trend evaluation of the studied locations from 1940 to 2023 based on the Mann–Kendall Tau coefficient.

Layout	Feature	Point number							
		Point 1	Point 2	Point 3	Point 4	Point 5	Point 6	Point 7	Point 8
Layout 1	Mean	0.4458	0.3620	0.4378	0.4452	0.1050	0.2605	0.6122	0.6816
	Median	0.4561	0.3832	0.4756	0.4177	0.0838	0.2456	0.6116	0.6517
	10th perc	0.4464	0.3115	0.3947	0.4527	0.2765	0.2616	0.5617	0.5978
	90th perc	0.3580	0.2656	0.3592	0.3976	−0.0098	0.1905	0.5743	0.6948
Layout 2	Mean	0.4441	0.3614	0.4395	0.4441	0.1056	0.2610	0.6116	0.6810
	Median	0.4573	0.3804	0.4756	0.4165	0.0820	0.2467	0.6139	0.6512
	10th perc	0.4492	0.3087	0.3964	0.4527	0.2760	0.2605	0.5611	0.5967
	90th perc	0.3580	0.2656	0.3620	0.3982	−0.0098	0.1905	0.5737	0.6948
Layout 3	Mean	0.4412	0.3609	0.4446	0.4464	0.1050	0.2599	0.6139	0.6810
	Median	0.4584	0.3815	0.4750	0.4171	0.0838	0.2444	0.6127	0.6506
	10th perc	0.4429	0.3098	0.4005	0.4515	0.2737	0.2628	0.5628	0.5967
	90th perc	0.3597	0.2633	0.3655	0.3959	−0.0126	0.1899	0.5731	0.6948
Layout 4	Mean	0.4423	0.3620	0.4400	0.4441	0.1044	0.2616	0.6122	0.6810
	Median	0.4544	0.3815	0.4756	0.4177	0.0838	0.2484	0.6133	0.6506
	10th perc	0.4458	0.3098	0.4010	0.4515	0.2754	0.2622	0.5611	0.5972
	90th perc	0.3574	0.2662	0.3614	0.3976	−0.0109	0.1905	0.5743	0.6948

Table 4
WEC layouts yearly capture width ratio (CWR) trend evaluation of the studied locations from 1940 to 2023 based on the Mann–Kendall Tau coefficient.

Layout	Feature	Point number							
		Point 1	Point 2	Point 3	Point 4	Point 5	Point 6	Point 7	Point 8
Layout 1	Mean	0.1102	0.2828	−0.1715	0.3741	−0.3442	−0.1956	−0.6219	−0.5473
	Median	−0.0981	0.2519	−0.3884	0.3936	−0.144	−0.202	−0.6219	−0.5123
	10th perc	0.3075	0.2467	0.3104	0.2616	−0.0585	0.031	−0.3775	0.5404
	90th perc	−0.0878	−0.2524	−0.2995	0.2587	−0.4114	−0.222	−0.5077	−0.5777
Layout 2	Mean	0.1159	0.2754	−0.1033	0.3775	−0.3511	−0.1813	−0.6208	−0.5427
	Median	−0.1038	0.2559	−0.3339	0.397	−0.1486	−0.1974	−0.6156	−0.5014
	10th perc	0.3069	0.2456	0.3178	0.2639	−0.0849	0.0356	−0.3655	0.5422
	90th perc	−0.0958	−0.2415	−0.3006	0.381	−0.4108	−0.2197	−0.5077	−0.5749
Layout 3	Mean	0.1073	0.2628	0.1228	0.3678	−0.3419	−0.1922	−0.6219	−0.5181
	Median	−0.0929	0.2433	−0.2553	0.3913	−0.1417	−0.2008	−0.6225	−0.4739
	10th perc	0.2995	0.2456	0.3781	0.2628	−0.0975	0.0327	−0.3517	0.5404
	90th perc	−0.0849	−0.1962	−0.2708	0.3735	−0.4102	−0.2255	−0.5077	−0.5772
Layout 4	Mean	0.1124	0.2742	−0.0654	0.3683	−0.3442	−0.1847	−0.6225	−0.5422
	Median	−0.0849	0.2582	−0.3511	0.3924	−0.1457	−0.2014	−0.619	−0.5181
	10th perc	0.3075	0.2427	0.3701	0.2628	−0.0958	0.0333	−0.3752	0.5404
	90th perc	−0.0889	−0.2347	−0.3052	0.3391	−0.4114	−0.2226	−0.5077	−0.5766

Table 5
WEC layouts yearly q-factor trend evaluation of the studied locations from 1940 to 2023 based on the Mann–Kendall Tau coefficient.

Layout	Feature	Point number							
		Point 1	Point 2	Point 3	Point 4	Point 5	Point 6	Point 7	Point 8
Layout 1	Mean	0.004	0.2874	−0.4228	0.3333	0.3339	−0.2398	−0.5915	−0.5955
	Median	0.0229	0.2587	−0.1951	0.3758	0.1997	−0.2278	−0.5743	−0.5525
	10th perc	0.2375	−0.0448	0.109	0.1211	0.1922	0.004	−0.0901	0.5055
	90th perc	−0.0356	−0.1377	−0.241	−0.3351	0.4177	0.2347	0.4923	0.5863
Layout 2	Mean	−0.0476	0.1377	−0.3723	0.3236	0.1274	0.1279	−0.4504	−0.5737
	Median	−0.0763	0.1916	0.105	0.3402	−0.1601	0.1073	−0.3844	−0.506
	10th perc	−0.0952	−0.1618	0.0333	0.2857	0.1406	−0.0207	0.5066	0.5508
	90th perc	−0.0218	−0.1119	−0.0534	0.3483	0.4131	0.2628	0.51	−0.0155
Layout 3	Mean	−0.1308	−0.2851	0.4269	0.3528	0.3414	0.1566	0.572	0.611
	Median	−0.0281	−0.2513	0.4601	0.3695	0.1647	0.1681	0.5863	0.5967
	10th perc	−0.0671	0.1561	−0.1578	0.0103	−0.0407	−0.0189	0.5582	−0.5376
	90th perc	0.1073	0.1824	0.3356	0.2702	−0.1698	0	0.5066	0.5818
Layout 4	Mean	−0.1113	−0.2507	0.1658	0.3832	0.3098	−0.1463	−0.5789	−0.5806
	Median	0.0241	−0.1561	0.4573	0.3855	0.1107	−0.144	−0.5181	−0.5399
	10th perc	0.1222	−0.1417	0.2341	0.2375	−0.1256	0.0327	0.1199	−0.3718
	90th perc	−0.1658	0.1509	−0.284	−0.3201	0.3901	0.1876	−0.0172	0.537

Table 6
WEC layouts seasonal mean total absorbed power (P_{avg}) trend evaluation of the studied locations from 1940 to 2023 based on the Mann–Kendall Tau coefficient.

Layout	Season	Point number							
		Point 1	Point 2	Point 3	Point 4	Point 5	Point 6	Point 7	Point 8
Layout 1	Winter	0.3465	0.2174	0.4905	0.4182	0.1515	0.1681	0.4435	0.5209
	Spring	0.3029	0.2106	0.3259	0.3052	0.0941	0.2123	0.5060	0.5634
	Summer	0.4217	0.2324	0.3769	0.3305	−0.0528	0.2335	0.5582	0.5686
	Autumn	0.3029	0.2392	0.4441	0.3597	0.0608	0.1371	0.5055	0.6294
Layout 2	Winter	0.3419	0.2174	0.4854	0.4194	0.1486	0.1692	0.4429	0.5215
	Spring	0.3092	0.2111	0.3276	0.3041	0.0947	0.2100	0.5037	0.5640
	Summer	0.4223	0.2341	0.3787	0.3305	−0.0528	0.2232	0.5594	0.5703
	Autumn	0.3046	0.2381	0.4441	0.3574	0.0602	0.1388	0.5066	0.6299
Layout 3	Winter	0.3396	0.2100	0.4911	0.4240	0.1549	0.1687	0.4464	0.5215
	Spring	0.3029	0.2088	0.3282	0.3035	0.0981	0.2123	0.5055	0.5582
	Summer	0.4188	0.2335	0.3792	0.3310	−0.0516	0.2238	0.5600	0.5680
	Autumn	0.3138	0.2398	0.4458	0.3580	0.0620	0.1406	0.5072	0.6299
Layout 4	Winter	0.3414	0.2146	0.4917	0.4234	0.1503	0.1692	0.4441	0.5209
	Spring	0.3110	0.2111	0.3282	0.3046	0.0941	0.2106	0.5049	0.5622
	Summer	0.4228	0.2335	0.3787	0.3310	−0.0534	0.2329	0.5594	0.5691
	Autumn	0.3035	0.2410	0.4446	0.3592	0.0591	0.1383	0.5066	0.6294

even decreasing CWR and q-factor trends. This finding suggests that an increase in raw absorbed power does not necessarily translate to improved efficiency metrics, which highlights the need for careful array design. To provide a quantitative perspective, the Mann–Kendall Tau coefficient trends for CWR across different locations and array layouts indicate significant variability. For instance, Layout 1 exhibits a mix of positive and negative trends, with Point 4 showing the highest positive mean trend (0.3741) while Point 7 exhibits the most pronounced decline (−0.6219). Similarly, Layout 2 follows a comparable pattern, with a strong positive trend at Point 4 (0.3775) but a notable decrease at Point 7 (−0.6208).

- **Climate Change Impact on Wave Patterns:** The results indicate that climate change is influencing wave patterns in ways that affect the performance of WECs. Increased wave energy availability was observed in some locations, aligning with global climate models predicting more energetic wave climates in certain regions. However, the impact is not uniform, and some areas show less consistent trends, which could be related to regional climate variability and oceanic circulation changes.

In conclusion, this research demonstrated that while climate change can enhance wave energy potential in certain areas, the performance of WEC arrays depends heavily on spatial considerations and array configuration. Not all locations or layouts benefit equally from changing wave conditions, with some arrays experiencing diminishing efficiency metrics despite increased absorbed power. Future WEC development should take into account the complex wave-structure interactions and consider location-specific trends to optimize power performance. As climate patterns continue to evolve, further research should focus on adaptive and resilient WEC designs that can capitalize on favorable trends while mitigating the impacts of destructive wave interference. Moreover, future studies could extend this analysis by incorporating long-term wave projections from CMIP6 climate models to assess how future climate scenarios may impact WEC power performance. This would enable a more comprehensive understanding of potential changes in wave energy resources and support the development of adaptive WEC array designs for future ocean conditions.

CRediT authorship contribution statement

Kumars Mahmoodi: Writing – review & editing, Writing – original draft, Visualization, Validation, Software, Resources, Methodology, Investigation, Formal analysis, Data curation, Conceptualization. **Hossein Rezaie Fard:** Writing – original draft, Visualization, Validation, Software. **Jari Böling:** Writing – review & editing, Funding acquisition.

Ethical approval

This paper is the author's original work and has not been previously published elsewhere.

Funding

This research is supported by the Business Finland project INDECS with grant number 7682/31/2022.

Declaration of competing interest

The authors declare that they have no conflicts of interest regarding the publication of this research article. The research was conducted in the absence of any commercial or financial relationships that could be construed as a potential conflict of interest.

Acknowledgments

We would like to extend our sincere gratitude to the Centre for Ocean Energy Research (COER) of Maynooth University for providing access to the Ansys software for WEC modeling. Moreover, we would like to express our sincere appreciation to the reviewers for their meticulous evaluation and invaluable feedback.

Appendix

Additional results supporting the findings of the research are provided in this part.

A.1. Figures

See Figs. A.1–A.5.

A.2. Tables

See Tables A.1 and A.2.

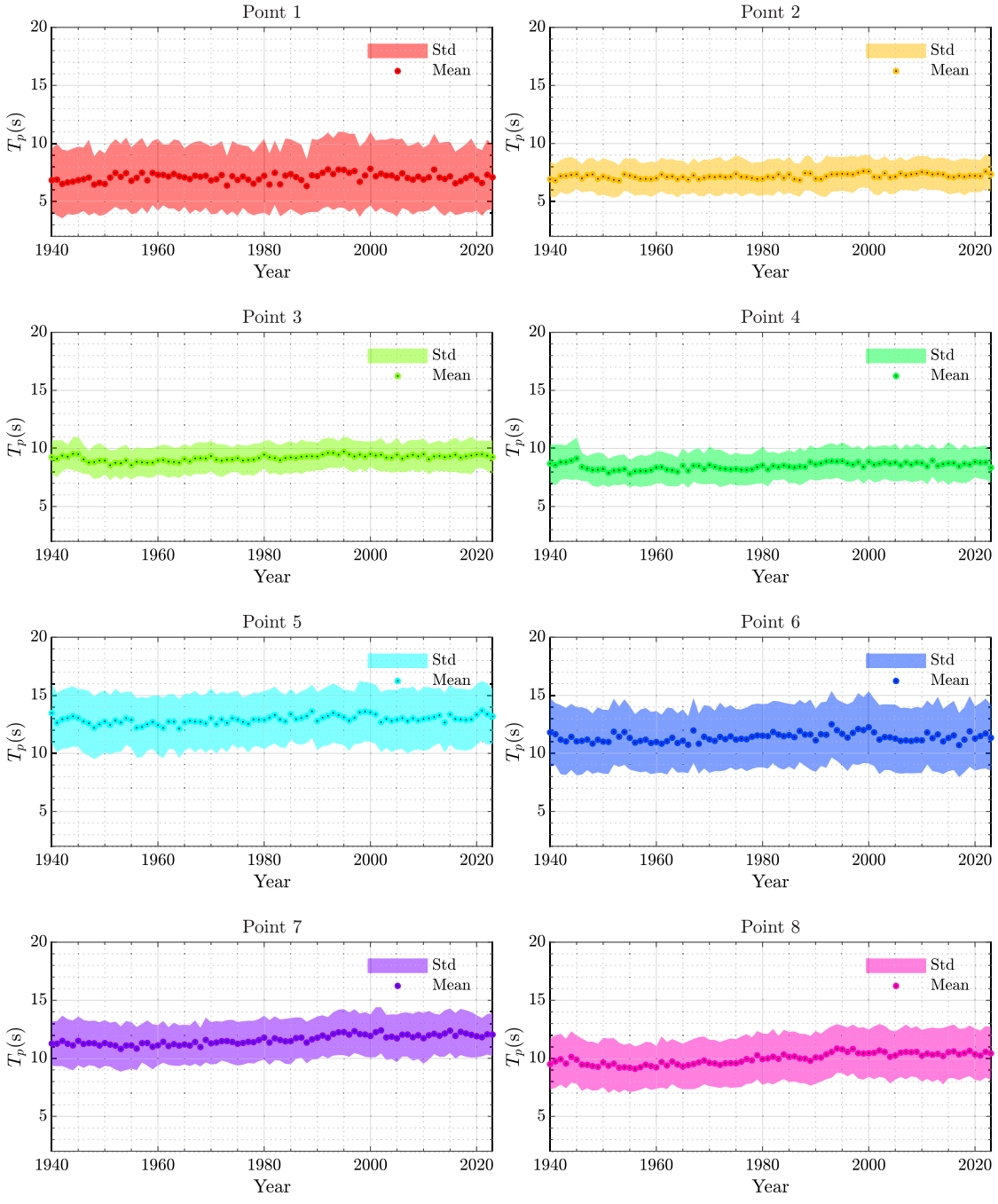

Fig. A.1. The overall yearly mean±std of T_p for the studied locations from 1940 to 2023.

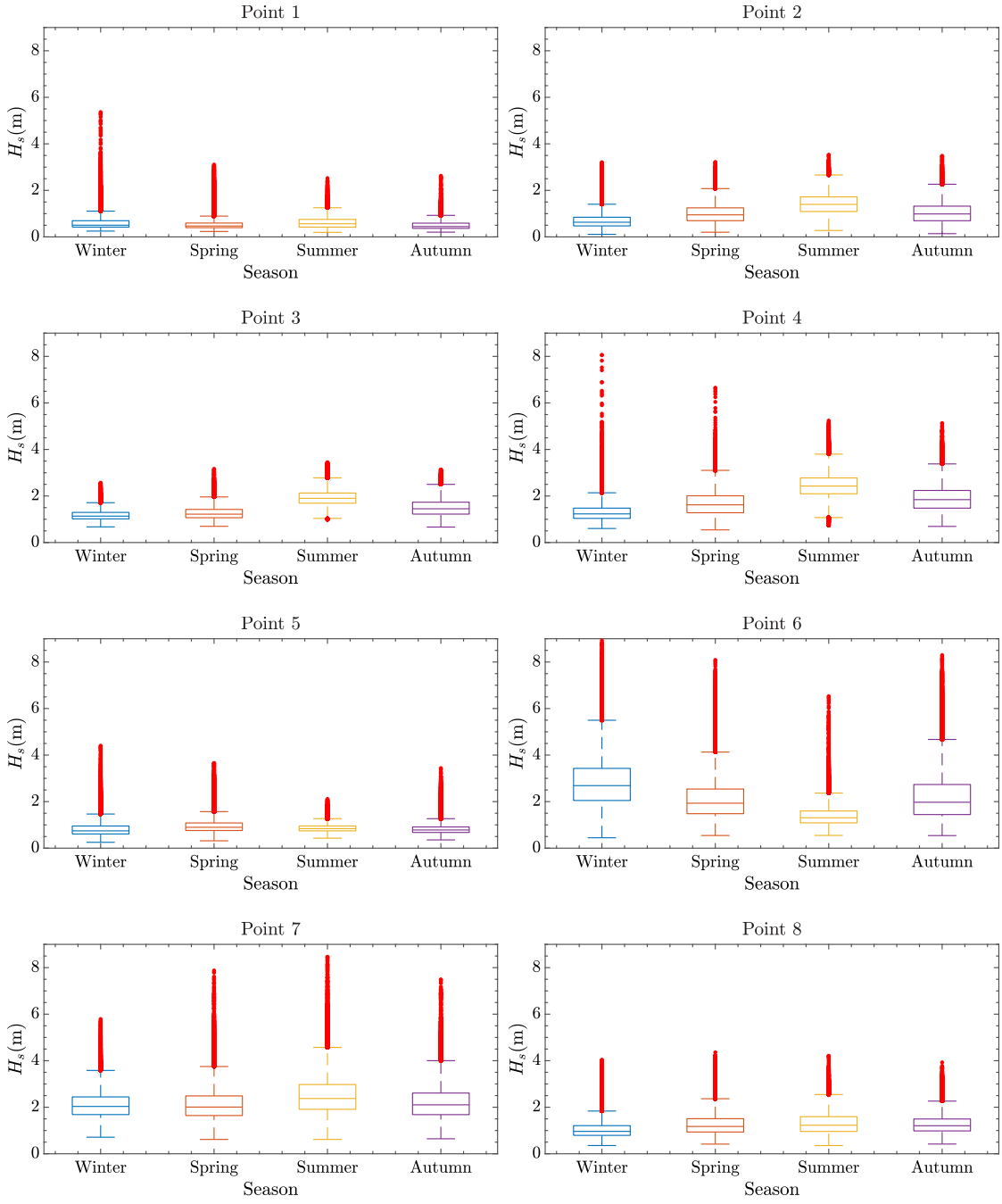

Fig. A.2. The overall seasonal mean boxplot of H_s for the studied locations from 1940 to 2023.

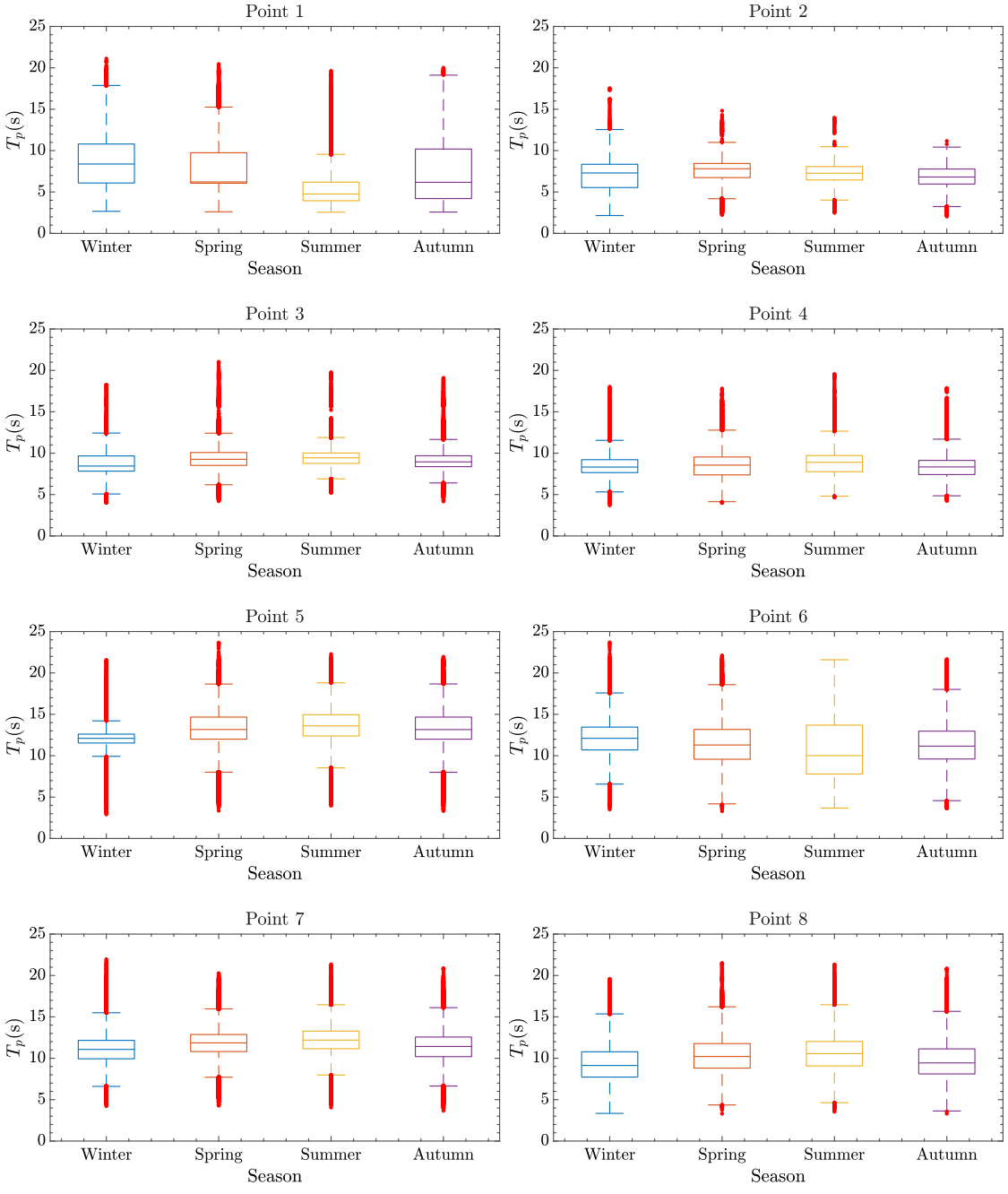

Fig. A.3. The overall seasonal mean boxplot of T_p for the studied locations from 1940 to 2023.

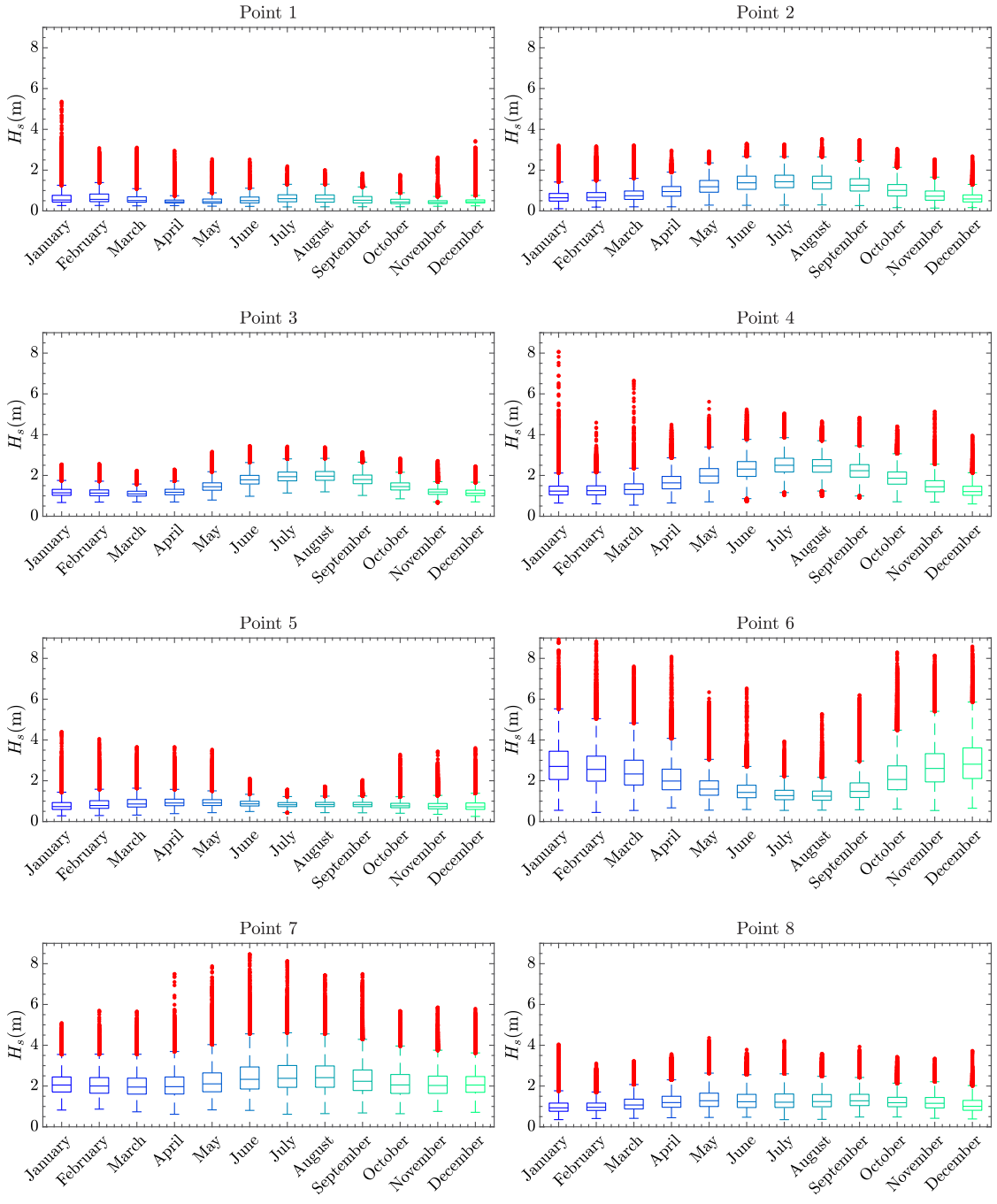

Fig. A.4. The overall monthly mean boxplot of H_s for the studied locations from 1940 to 2023.

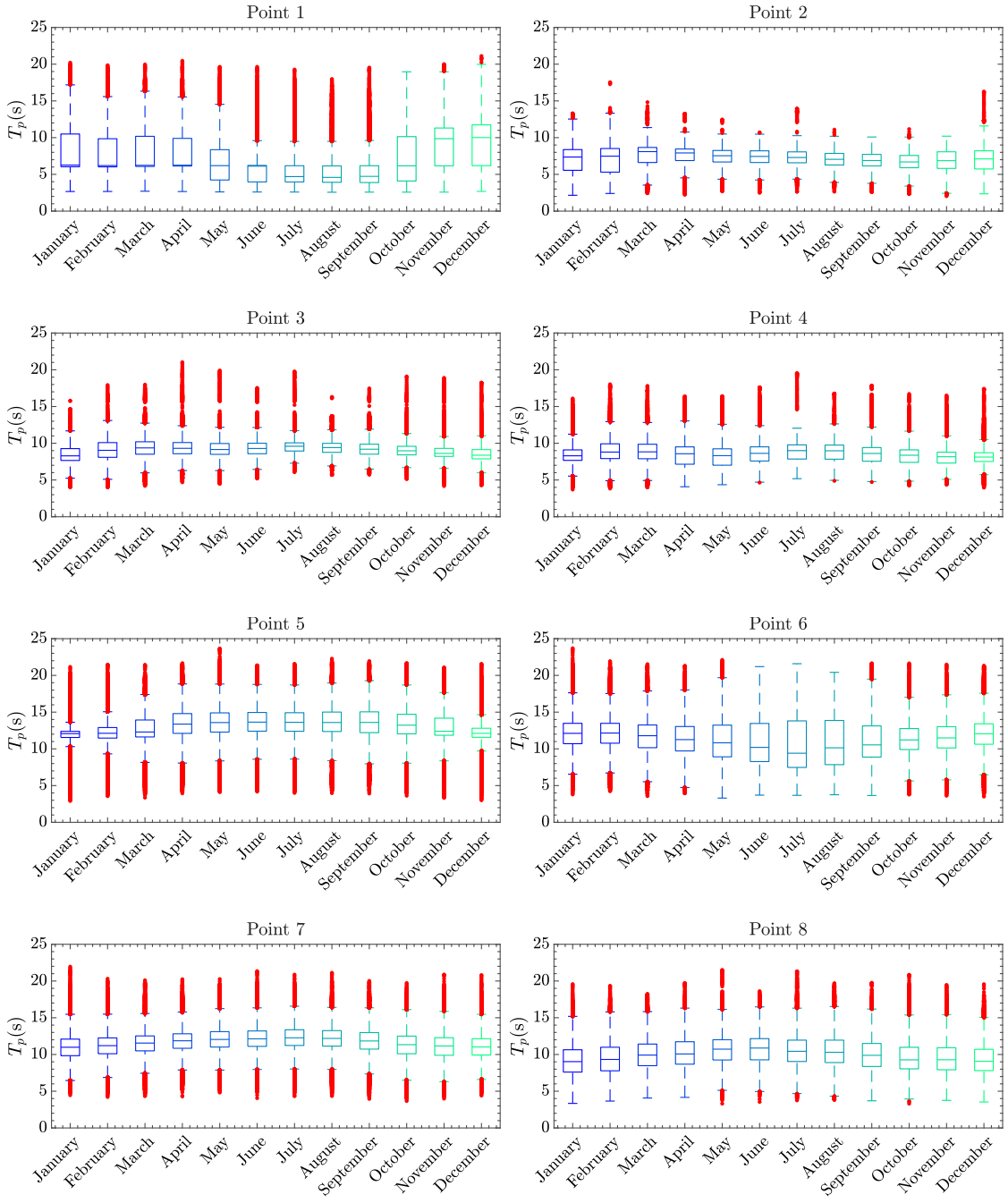

Fig. A.5. The overall monthly mean boxplot of T_p for the studied locations from 1940 to 2023.

Table A.1
WEC layouts seasonal mean capture width ratio (CWR) trend evaluation of the studied locations from 1940 to 2023 based on the Mann–Kendall Tau coefficient.

Layout	Season	Point number							
		Point 1	Point 2	Point 3	Point 4	Point 5	Point 6	Point 7	Point 8
Layout 1	Winter	0.1291	0.1979	0.2737	0.3454	−0.3391	−0.3878	−0.3523	0.1124
	Spring	0.2312	0.21	−0.039	0.3087	−0.2823	−0.21	−0.5628	0.0293
	Summer	0.0138	0.1876	−0.179	0.2433	−0.1933	0.0838	−0.4808	−0.035
	Autumn	−0.0855	0.1354	−0.0534	0.2398	−0.1343	−0.1308	−0.3936	0.109
Layout 2	Winter	0.1354	0.1991	0.2783	0.3351	−0.3282	−0.3792	−0.3373	0.1572
	Spring	0.2433	0.2083	0.0298	0.311	−0.28	−0.1652	−0.5588	−0.0189
	Summer	0.0092	0.1888	−0.1664	0.2387	−0.1968	0.0683	−0.4722	−0.0671
	Autumn	−0.0895	0.1354	−0.0201	0.2369	−0.1337	−0.066	−0.3781	0.1549
Layout 3	Winter	0.1239	0.2014	0.2737	0.3511	−0.3316	−0.3666	−0.0252	0.4303
	Spring	0.2593	0.2025	0.1583	0.2937	−0.2817	−0.1515	−0.5674	0.3672
	Summer	0.0075	0.1899	0.1004	0.2507	−0.1916	0.0373	−0.4699	0.2565
	Autumn	−0.0901	0.1365	0.1721	0.2387	−0.1343	−0.0947	−0.3253	0.4842
Layout 4	Winter	0.1216	0.2008	0.2725	0.3454	−0.3305	−0.3844	−0.2083	0.2496
	Spring	0.2593	0.2083	0.0235	0.3035	−0.2806	−0.1721	−0.5594	0.1956
	Summer	0.0155	0.1882	−0.1015	0.2444	−0.1945	0.0769	−0.4745	0.0803
	Autumn	−0.0906	0.136	−0.0149	0.2392	−0.1337	−0.0792	−0.3551	0.2444

Table A.2
WEC layouts seasonal mean q-factor trend evaluation of the studied locations from 1940 to 2023 based on the Mann–Kendall Tau coefficient.

Layout	Season	Point number							
		Point 1	Point 2	Point 3	Point 4	Point 5	Point 6	Point 7	Point 8
Layout 1	Winter	0.1417	0.2083	0.1314	0.2651	0.0688	0.0493	−0.5003	−0.3184
	Spring	0.0734	0.2238	−0.2054	0.2874	0.2622	−0.1337	−0.311	−0.4527
	Summer	−0.0608	0.1979	−0.3328	0.1572	0.2197	0.074	0.3046	−0.4509
	Autumn	0.0476	0.1084	−0.1411	0.2501	0.1325	−0.1647	−0.4716	−0.5393
Layout 2	Winter	0.1285	0.2111	0.1199	−0.0723	−0.1102	0.1234	−0.4877	−0.1526
	Spring	−0.0052	0.07	−0.012	0.1675	0.2014	−0.101	0.4372	−0.4527
	Summer	−0.0516	0.2215	−0.2725	0.109	0.1492	0.0201	0.4733	−0.4532
	Autumn	0.0321	0.117	0.0407	0.0797	0.1015	0.0499	−0.1962	−0.4601
Layout 3	Winter	−0.0293	−0.1538	0.2513	0.1853	0.3276	0.3741	0.5106	0.5175
	Spring	−0.1905	−0.2243	0.3133	0.1434	0.2679	0.2065	0.5347	0.4785
	Summer	−0.0516	−0.1847	0.3178	0.226	0.2932	−0.1107	0.467	0.455
	Autumn	0.039	−0.0878	0.3546	0.0069	0.1377	0.117	0.4452	0.5571
Layout 4	Winter	0.0998	−0.0912	0.3081	0.2708	0.0522	0.2547	−0.5032	0.1463
	Spring	0.1067	0.0419	0.1216	0.2645	0.2697	−0.1365	0.4664	−0.4613
	Summer	−0.0499	−0.1807	0.0711	0.2392	0.1446	0.0872	0.459	−0.4618
	Autumn	0.0126	0.0189	0.358	0.2232	0.1256	−0.113	−0.3069	−0.3035

Data availability

Data will be made available on request.

References

[1] Pourali M, Kavianpour MR, Kamranzad B, Alizadeh MJ. Future variability of wave energy in the Gulf of Oman using a high resolution CMIP6 climate model. Energy 2023;262:125552. http://dx.doi.org/10.1016/j.energy.2022.125552, URL: https://www.sciencedirect.com/science/article/pii/S0360544222024380.

[2] Xu X, Sasmal K, Wen Y, Xu H, Ma P, Tkalich P, et al. An integrated approach for the decision of wave energy converter deployment based on forty-five-years high-resolution wave climate modeling. Energy 2024;305:132238. http://dx.doi.org/10.1016/j.energy.2024.132238, URL: https://www.sciencedirect.com/science/article/pii/S0360544224020127.

[3] Mahmoodi K. Ocean wave energy resources. In: Reference module in earth systems and environmental sciences. Elsevier; 2024, http://dx.doi.org/10.1016/B978-0-323-93940-9.00194-8, URL: https://www.sciencedirect.com/science/article/pii/B9780323939409001948.

[4] Ermakov AM, Ali ZA, Mahmoodi K, Mason O, Ringwood JV. Optimisation of heterogeneous wave energy converter arrays: A control co-design strategy. Renew Energy 2025;244:122637. http://dx.doi.org/10.1016/j.renene.2025.122637, URL: https://www.sciencedirect.com/science/article/pii/S096014812500299X.

[5] Arguilé-Pérez B, Ribeiro A, Costoya X, deCastro M, Gómez-Gesteira M. Suitability of wave energy converters in northwestern Spain under the near future winter wave climate. Energy 2023;278:127957. http://dx.doi.org/10.1016/j.energy.2023.127957, URL: https://www.sciencedirect.com/science/article/pii/S0360544223013518.

[6] Mahmoodi K, Ghassemi H, Razminia A. Performance assessment of a two-body wave energy converter based on the Persian Gulf wave climate. Renew Energy 2020;159:519–37. http://dx.doi.org/10.1016/j.renene.2020.06.071, URL: https://www.sciencedirect.com/science/article/pii/S0960148120309812.

[7] Sun P, Wang J. Long-term variability analysis of wave energy resources and its impact on wave energy converters along the Chinese coastline. Energy 2024;288:129644. http://dx.doi.org/10.1016/j.energy.2023.129644, URL: https://www.sciencedirect.com/science/article/pii/S0360544223030384.

[8] Ermakov A, Ali ZA, Mahmoodi K, Mason O, Ringwood JV. A frequency domain-based control methodology for performance assessment and optimisation of heterogeneous arrays of wave energy converters. In: 2024 IEEE Conference on control technology and applications. 2024, p. 584–9. http://dx.doi.org/10.1109/CCTA60707.2024.10666578.

[9] Xu J, Li J, Pan S, Yao Y, Chen L, Wu Z. Assessment of wind and wave energy in China seas under climate change based on CMIP6 climate model. Energy 2024;310:133207. http://dx.doi.org/10.1016/j.energy.2024.133207, URL: https://www.sciencedirect.com/science/article/pii/S0360544224029827.

[10] Solaun K, Cerdá E. Climate change impacts on renewable energy generation. A review of quantitative projections. Renew Sustain Energy Rev 2019;116:109415. http://dx.doi.org/10.1016/j.rser.2019.109415, URL: https://www.sciencedirect.com/science/article/pii/S1364032119306239.

[11] Oleinik PH, Maciel RP, dos Santos ED, Rocha LAO, Machado BN, Isoldi LA. Numerical method for the characterization of sea states using realistic irregular waves on computational fluid dynamics simulations for application on wave energy converters. Sustain Energy Technol Assess 2025;73:104093. http://dx.doi.org/10.1016/j.seta.2024.104093, URL: https://www.sciencedirect.com/science/article/pii/S2213138824004892.

[12] Islek F, Yuksel Y. Possible changes and occurrences of future wave power in an enclosed sea using a high-resolution regional climate model. Ocean Eng 2024;303:117843. http://dx.doi.org/10.1016/j.oceaneng.2024.117843, URL: https://www.sciencedirect.com/science/article/pii/S0029801824011818.

[13] Mahmoodi K, Saybani M, Azad ST. A temporal and spatial resolution wind and wave power resource assessment in the Oman Gulf. Ocean Eng 2022;249:110881. http://dx.doi.org/10.1016/j.oceaneng.2022.110881, URL: https://www.sciencedirect.com/science/article/pii/S0029801822003213.

[14] Mahmoodi K, Ghassemi H, Razminia A. Temporal and spatial characteristics of wave energy in the Persian Gulf based on the ERA5 reanalysis dataset. Energy 2019;187:115991.

[15] Ulazia A, Saenz-Aguirre A, Ibarra-Berastegui G, Sáenz J, Carreno-Madinabeitia S, Esnaola G. Performance variations of wave energy converters due to global long-term wave period change (1900–2010). Energy 2023;268:126632. http://dx.doi.org/10.1016/j.energy.2023.126632, URL: https://www.sciencedirect.com/science/article/pii/S0360544223000269.

[16] deCastro M, Rusu L, Arguilé-Pérez B, Ribeiro A, Costoya X, Carvalho D, et al. Different approaches to analyze the impact of future climate change on the exploitation of wave energy. Renew Energy 2024;220:119569. http://dx.doi.org/10.1016/j.renene.2023.119569, URL: https://www.sciencedirect.com/science/article/pii/S0960148123014842.

[17] Appendini CM, Ruiz-Salcines P, Marsooli R, Cerezo-Mota R. Assessing the effects of climate change on the Gulf of Mexico wave climate using the COWCLIP framework and the PRECIS regional climate model. Ocean Model 2025;194:102486. http://dx.doi.org/10.1016/j.ocemod.2024.102486, URL: https://www.sciencedirect.com/science/article/pii/S1463500324001720.

[18] Simonetti I, Cappietti L. Mediterranean coastal wave-climate long-term trend in climate change scenarios and effects on the optimal sizing of OWC wave energy converters. Coast Eng 2023;179:104247. http://dx.doi.org/10.1016/j.coastaleng.2022.104247, URL: https://www.sciencedirect.com/science/article/pii/S0378383922001600.

[19] Iglesias G, Abanades J. Wave power: Climate change mitigation and adaptation. In: Handbook of climate change mitigation and adaptation. Cham: Springer International Publishing; 2017, p. 2007–55. http://dx.doi.org/10.1007/978-3-319-14409-2_81.

[20] Shukla J, Verma M, Misra A. Effect of global warming on sea level rise: A modeling study. Ecol Complex 2017;32:99–110. http://dx.doi.org/10.1016/j.ecocom.2017.10.007, URL: https://www.sciencedirect.com/science/article/pii/S1476945X17300910.

[21] Qu Y, Liu Y, Jevrejeva S, Jackson LP. Future sea level rise along the coast of China and adjacent region under 1.5 °C and 2.0 °C global warming. Adv Clim Chang Res 2020;11(3):227–38. http://dx.doi.org/10.1016/j.accre.2020.09.001, Including special topic on East Asian climate response to 1.5/2 °C global warming, URL: https://www.sciencedirect.com/science/article/pii/S1674927820300642.

[22] Lavidas G, Blok K. Shifting wave energy perceptions: The case for wave energy converter (WEC) feasibility at milder resources. Renew Energy 2021;170:1143–55. http://dx.doi.org/10.1016/j.renene.2021.02.041, URL: https://www.sciencedirect.com/science/article/pii/S0960148121002093.

[23] Penalba M, Ulazia A, Saénz J, Ringwood JV. Impact of long-term resource variations on wave energy farms: The Icelandic case. Energy 2020;192:116609. http://dx.doi.org/10.1016/j.energy.2019.116609, URL: https://www.sciencedirect.com/science/article/pii/S0360544219323047.

[24] Reeve D, Chen Y, Pan S, Magar V, Simmonds D, Zacharioudaki A. An investigation of the impacts of climate change on wave energy generation: The Wave Hub, Cornwall, UK. Renew Energy 2011;36(9):2404–13. http://dx.doi.org/10.1016/j.renene.2011.02.020, URL: https://www.sciencedirect.com/science/article/pii/S096014811100111X.

[25] Hemer M, Fan Y, Mori N, Semedo A, Wang X. Projected changes wave climate from a multi-model ensemble. Nat Clim Chang 2013. http://dx.doi.org/10.1038/NCLIMATE1791.

[26] Reguero B, Losada I, Mendez F. A recent increase in global wave power as a consequence of oceanic warming. Nat Commun 2019;10. http://dx.doi.org/10.1038/s41467-018-08066-0.

[27] Penalba M, Ulazia A, Ibarra-Berastegui G, Ringwood J, Sáenz J. Wave energy resource variation off the west coast of Ireland and its impact on realistic wave energy converters' power absorption. Appl Energy 2018;224:205–19. http://dx.doi.org/10.1016/j.apenergy.2018.04.121, URL: https://www.sciencedirect.com/science/article/pii/S0306261918306895.

[28] Olabi A, Abdelkareem MA. Renewable energy and climate change. Renew Sustain Energy Rev 2022;158:112111. http://dx.doi.org/10.1016/j.rser.2022.112111, URL: https://www.sciencedirect.com/science/article/pii/S1364032122000405.

[29] Majidi AG, Ramos V, Giannini G, Rosa Santos P, das Neves L, Taveira-Pinto F. The impact of climate change on the wave energy resource potential of the Atlantic Coast of Iberian Peninsula. Ocean Eng 2023;284:115451. http://dx.doi.org/10.1016/j.oceaneng.2023.115451, URL: https://www.sciencedirect.com/science/article/pii/S0029801823018358.

[30] Liu J, Li R, Li S, Meucci A, Young IR. Increasing wave power due to global climate change and intensification of Antarctic oscillation. Appl Energy 2024;358:122572. http://dx.doi.org/10.1016/j.apenergy.2023.122572, URL: https://www.sciencedirect.com/science/article/pii/S0306261923019360.

[31] Sarkar S, Gundecha V, Ghorbanpour S, ramesh babu A, Pichard A, Cocho M. Skip training for multi-agent reinforcement learning controller for industrial wave energy converters. 2022, http://dx.doi.org/10.48550/arXiv.2209.05656.

[32] Al Shami E, Wang X. Performance prediction and design parameters sensitivity analysis of two-body point absorber wave energy harvesters. Ocean Eng 2023;286:115538. http://dx.doi.org/10.1016/j.oceaneng.2023.115538, URL: https://www.sciencedirect.com/science/article/pii/S0029801823019224.

[33] Wildan Amarullah A, Kurniawan TW, Yanuar N, Sholahudin Ario G, Yong Z. Hydrodynamic performance and multi-objective optimization of multi-cylinder floating point absorber wave energy converter. Ocean Eng 2025;317:120040. http://dx.doi.org/10.1016/j.oceaneng.2024.120040, URL: https://www.sciencedirect.com/science/article/pii/S002980182403378X.

[34] Shadmani A, Nikoo MR, Gandomi AH, Wang R-Q, Golparvar B. A review of machine learning and deep learning applications in wave energy forecasting and WEC optimization. Energy Strat Rev 2023;49:101180. http://dx.doi.org/10.1016/j.esr.2023.101180, URL: https://www.sciencedirect.com/science/article/pii/S2211467X2300130X.

[35] Wu H, Liang Y, Gao X-Z. Left-right brain interaction inspired bionic deep network for forecasting significant wave height. Energy 2023;278:127995. http://dx.doi.org/10.1016/j.energy.2023.127995, URL: https://www.sciencedirect.com/science/article/pii/S0360544223013890.

[36] Ouyang Z, Zhao Y, Zhang D, Zhang X. An effective deep learning model for spatial-temporal significant wave height prediction in the Atlantic hurricane area. Ocean Eng 2025;317:120083. http://dx.doi.org/10.1016/j.oceaneng.2024.120083, URL: https://www.sciencedirect.com/science/article/pii/S0029801824034218.

[37] Chen J, Li S, Zhu J, Liu M, Li R, Cui X, et al. Significant wave height prediction based on variational mode decomposition and dual network model. Ocean Eng 2025;323:120533. http://dx.doi.org/10.1016/j.oceaneng.2025.120533, URL: https://www.sciencedirect.com/science/article/pii/S0029801825002483.

[38] Li D, Wang T, Tao J, Sharma S, Borthwick AG, Dong X, et al. Model predictive control of a single-buoy wave energy converter with coupled constraints and model adaptation. Ocean Eng 2025;315:119887. http://dx.doi.org/10.1016/j.oceaneng.2024.119887, URL: https://www.sciencedirect.com/science/article/pii/S0029801824032256.

[39] Neshat M, Sergiienko NY, Rafiee A, Mirjalili S, Gandomi AH, Boland J. Meta Wave Learner: Predicting wave farms power output using effective meta-learner deep gradient boosting model: A case study from Australian coasts. Energy 2024;304:132122. http://dx.doi.org/10.1016/j.energy.2024.132122, URL: https://www.sciencedirect.com/science/article/pii/S0360544224018966.

[40] Liang H, Qin H, Su H, Wen Z, Mu L. Environmental-sensing and adaptive optimization of wave energy converter based on deep reinforcement learning and computational fluid dynamics. Energy 2024;297:131254. http://dx.doi.org/10.1016/j.energy.2024.131254, URL: https://www.sciencedirect.com/science/article/pii/S0360544224010272.

[41] Clemente D, Teixeira-Duarte F, Rosa-Santos P, Taveira-Pinto F. Advancements on optimization algorithms applied to wave energy assessment: An overview on wave climate and energy resource. Energies 2023;16(12). http://dx.doi.org/10.3390/en16124660, URL: https://www.mdpi.com/1996-1073/16/12/4660.

[42] Copernicus Climate Change Service CDS. ERA5 hourly data on single levels from 1940 to present. Copernicus Climate Change Service (C3S) Climate Data Store (CDS); 2024, http://dx.doi.org/10.24381/cds.adbb2d47, [Accessed 12 October 2024].

[43] Mahmoodi K, Razminia A, Ghassemi H. Optimal control of wave energy converters with non-integer order performance indices: A dynamic programming approach. Renew Energy 2021;177:1212–33. http://dx.doi.org/10.1016/j.renene.2021.06.045, URL: https://www.sciencedirect.com/science/article/pii/S0960148121009113.

[44] Chen M, Deng J, Yang Y, Zhou H, Tao T, Liu S, et al. Performance analysis of a floating wind–wave power generation platform based on the frequency domain model. J Mar Sci Eng 2024;12(2). http://dx.doi.org/10.3390/jmse12020206, URL: https://www.mdpi.com/2077-1312/12/2/206.

[45] Penalba M, Giorgi G, Ringwood JV. Mathematical modelling of wave energy converters: A review of nonlinear approaches. Renew Sustain Energy Rev 2017;78:1188–207. http://dx.doi.org/10.1016/j.rser.2016.11.137, URL: https://www.sciencedirect.com/science/article/pii/S1364032116308784.

[46] Ermakov A, Ali ZA, Mahmoodi K, Mason O, Ringwood JV. A frequency domain-based control methodology for performance assessment and optimisation of heterogeneous arrays of wave energy converters. In: 2024 IEEE conference on control technology and applications. 2024, p. 584–9. http://dx.doi.org/10.1109/CCTA60707.2024.10666578.

[47] Mahmoodi K, Nepomuceno E, Razminia A. Wave excitation force forecasting using neural networks. Energy 2022;247:123322. http://dx.doi.org/10.1016/j.energy.2022.123322, URL: https://www.sciencedirect.com/science/article/pii/S0360544222002250.

[48] Pereira D. Wind rose. 2024, https://www.mathworks.com/matlabcentral/fileexchange/47248-wind-rose, MATLAB Central File Exchange. Retrieved August 8, 2024.

[49] Kamal N, Pachauri S, et al. Mann-Kendall test—A novel approach for statistical trend analysis. Int J Comput Trends Technol 2018;63:18–21. http://dx.doi.org/10.14445/22312803/IJCTT-V63P104.

[50] Hu Z, Liu S, Zhong G, Lin H, Zhou Z. Modified Mann-Kendall trend test for hydrological time series under the scaling hypothesis and its application. Hydrol Sci J 2020;65(14):2419–38. http://dx.doi.org/10.1080/02626667.2020.1810253, arXiv:https://doi.org/10.1080/02626667.2020.1810253.